SC5320.5FR

SC5320.5FR

Copy No. 16

STUDIES OF ABSORPTION IN SALT

FINAL REPORT FOR THE PERIOD
December 1, 1981 through November 30, 1982

CONTRACT NO. F49620-82-C-0015
DARPA ORDER NO. 4400

B.R. Tittmann
Principal Investigator
(805) 498-4545

Prepared for

Air Force Office of Scientific Research
Bolling Air Force Base
Washington, DC 20332

Sponsored by
Advanced Research Projects Agency (DOD)
DARPA Order No. 4400
Monitored by AFOSR Under Contract No. F49620-82-C-0015

FEBRUARY 1983

Rockwell International
Science Center

UNCLASSIFIED

SECURITY CLASSIFICATION OF THIS PAGE (When Data Entered)

REPORT DOCUMENTATION PAGE

READ INSTRUCTIONS BEFORE COMPLETING FORM

1. REPORT NUMBER: AFOSR-TR- 83-0682	2. GOVT ACCESSION NO.: AD-A131 670
3. RECIPIENT'S CATALOG NUMBER:	
4. TITLE (and Subtitle): STUDIES OF ABSORPTION IN SALT	5. TYPE OF REPORT & PERIOD COVERED: FINAL 1 Dec 81 - 30 Nov 82
	6. PERFORMING ORG. REPORT NUMBER:
7. AUTHOR(s): B. R. Tittmann	8. CONTRACT OR GRANT NUMBER(s): F49620-82-C-0015
9. PERFORMING ORGANIZATION NAME AND ADDRESS: Rockwell International, 1049 Camino Dos Rios, PO Box 1085, Thousand Oaks, CA 91360	10. PROGRAM ELEMENT, PROJECT, TASK AREA & WORK UNIT NUMBERS: 62147E, 2309/A1 (DARPA)
11. CONTROLLING OFFICE NAME AND ADDRESS: DARPA, 1400 Wilson Boulevard, Arlington, VA 22209	12. REPORT DATE: February 1983
	13. NUMBER OF PAGES: 45
14. MONITORING AGENCY NAME & ADDRESS (if different from Controlling Office): AFOSR/NP, Building 410, Bolling AFB DC 20332	15. SECURITY CLASS. (of this report): UNCLASSIFIED
	15a. DECLASSIFICATION DOWNGRADING SCHEDULE:

16. DISTRIBUTION STATEMENT (of this Report)

Approved for public release; distribution unlimited.

17. DISTRIBUTION STATEMENT (of the abstract entered in Block 20, if different from Report)

18. SUPPLEMENTARY NOTES

19. KEY WORDS (Continue on reverse side if necessary and identify by block number)

20. ABSTRACT (Continue on reverse side if necessary and identify by block number)

As result of recent studies, it has become apparent that most available data on free-field particle motion associated with underground chemical and nuclear explosions exhibit nonelastic behavior even at rather large scaled distances from the source. This observation casts suspicion on the usefulness of reduced displacement potential (RDP) calculations based upon these close range data for the purpose of defining a seismic source function (Bache et al, 1981). Experimental measurements on sandstone and igneous rocks indicate significant nonlinearty at intermediate strain amplitudes 10^{-4} and 10^{-6}.

DD FORM 1 JAN 73 1473 EDITION OF 1 NOV 65 IS OBSOLETE

UNCLASSIFIED

SECURITY CLASSIFICATION OF THIS PAGE (When Data Entered)

TABLE OF CONTENTS

LIST OF FIGURES

LIST OF FIGURES (continued)

1.0 SUMMARY AND INTRODUCTION

As result of recent studies (Trulio 1978, 1981), it has become apparent that most available data on free-field particle motion associated with underground chemical and nuclear explosions exhibit nonelastic behavior even at rather large scaled distances from the source. This observation casts suspicion on the usefulness of reduced displacement potential (RDP) calculations based upon these close range data for the purpose of defining a seismic source function (Bache et al, 1981). Experimental measurements on sandstones and igneous rocks indicate significant nonlinearity at intermediate strain amplitudes between 10^{-4} and 10^{-6} (Johnston and Toksoz, 1980; Mavko, 1979; Tittmann et al, 1982; Winkler et al, 1979). In this study we have used resonant bar-type measurements to study the transition from linear to nonlinear behavior in pressed salt and natural halite. These measurements are relevant to interpretive studies of the observed decay of peak particle velocity and displacement with scaled distance from the Cowboy series of explosions in dome salt. This study also complements the laboratory study by Larson (1981) of particle motions associated with small-scale chemical explosions in pressed salt.

Laboratory and field data outline the following scenario for material behavior as a function of scaled distance from the source.

1) At very close ranges, wave propagation is strongly nonlinear and non-elastic owing to such strongly nonreversible processes as shear failure, cracking, spalling, pore collapse, melting, and phase transformations.

2) At intermediate scaled distances near-linearity can be demonstrated, at least in the case of pressed salt (Larson, 1981), by showing the linear additivity of two signals produced by two simultaneous explosive charges. However, as described in this report, Q known to be amplitude-dependent in this regime,

indicating that the material is not exhibiting truly linear anelastic behavior.

3 At very great distance, attenuation is independent of strain amplitude, indicating linear anelastic behavior characteristic of teleseismic waves.

The transition from domain 1 to domain 2 can, in principle, be mapped in the manner described by Larson (1981) by examining the additivity of particle velocity. Attenuation within the nonlinear domain 2 and the transition from domain 2 to the seismic (linear anelastic) domain 3 can be mapped in the laboratory using the resonant bar-type instrument as described in this report.

Prior to this study the behavior of salt in the transition zone between strain amplitudes of 10^{-8} and 10^{-3} had not been investigated. It was the purpose of this investigation to increase our understanding of material behavior in the transition zone between the linear anelastic regime and the nonlinear nonelastic regime for both pressed salt and natural dome salt under a variety of environmental conditions most likely to be encountered in the field.

The experimental results described in this report indicate that natural dome salt is rather ideally behaved. At elevated effective pressures linear anelastic behavior is observed at strain amplitudes below about 2×10^{-6}, corresponding to stresses of about 1 bar. The linear anelastic Q for natural dome salt is quite high (~ 500 in extension and ~ 1000 in torsion), apparently independent of pressure up to 6.8×10^{7} Pa, and very slightly dependent on frequency between ~ 80 Hz and ~ 480 Hz. Nonlinear behavior, as reflected in an amplitude dependent Q, is observed at strain amplitudes above 2×10^{-6}, at all effective pressures to 6.8×10^{7} Pa (corresponding to burial depths of about 2.4 km). The observed departure from linear behavior in dome salt at strain amplitudes higher than 2×10^{-6} (~ 1

bar stress) indicates that RDP studies based upon particle motion measurements at higher amplitudes may not be useful for defining a seismic source function. The behavior of pressed salt contrasts with that of natural dome salt. Weakly nonlinear behavior persists to very low amplitudes (below 10^{-8}), corresponding to stresses of approximately 0.01 bars. Strongly nonlinear behavior is observed at strain amplitudes higher than 10^{-6}. Attenuation in pressed salt is frequency dependent. Under ambient pressure conditions attenuation is also sensitive to the amount of moisture adsorbed on internal cracks within the sample.

The microstructure of both types of salt is described. The most obvious difference between pressed salt and natural dome salt is in the grain size. The grains in the pressed salt are more than a decade smaller than the grains in the dome salt. This corresponds to at least a two decade difference in grain surface to volume ratio. These microstructural differences combined with the observed difference in the Q behavior of both types of salt cast suspicion on the use of pressed salt as a good mechanical analog for natural dome salt.

2.0 PETROGRAPHIC ANALYSIS OF SALT

Two types of samples are used in this study: a pressed salt sample provided by Donald Larson of Lawrence Livermore Laboratory and a natural salt block obtained from the Kleer mine at a depth of 750 ft. in the Grand Saline salt dome of eastern Texas. The pressed salt has a fine grain size (<1.3 mm) and was pressed in a cylindrical block at 1.4×10^8 Pa and 120°C for 1 hour. The natural halite contains grains which are an order of magnitude larger ($\lesssim$ 15 mm). A more comprehensive description of sample petrofabrics follows.

2.1 Microstructure of Salt

Considerable progress has been made in developing techniques to characterize the microstructure of the salt samples. The most important parameters are: a) the grain size distribution, b) crack size and density, and c) preferred orientation of grains or cracks. The results reported here were made on grab samples of both types of salt. Specimens are not documented as to orientation or location within the source blocks and may not be totally representative. The samples were studied with the following objectives in mind:

1. Develope a technique for crack decoration, enhancing grain boundaries and cracks for petrofabric studies.

2. Apply the Quantimet 900 Image analyzer to obtain statistical data on grain size distribution and crack density from photomicrographs.

3. Obtain microstructural data on samples and apply necessary corrections to derive volumetric data from the two dimensional measurements obtained from the photomicrographs.

2.2 Sample Preparation

Small slabs were saw cut about 3 cm thick and trimmed to conveniently fit on the microscope stage. Because the pressed salt is fine-grained (mm size) the slab was trimmed to about 3 cm on the side. In the case of the natural salt which has a gain diameter in excess of 1 cm a rectangular slab measuring 15 × 25 cm was prepared. The surface selected for study was hand polished to 8 μm. On the finished surface the grain boundaries and large cracks in the natural salt were clearly visible with the naked eye but photomicrographs with sufficient contrast could not be obtained.

2.3 Crack Decoration

We found that the most effective method to enhance the grain boundaries and cracks in salt is to use a fluorescent yellow dye with a petroleum base. The commercially available Zyglo dye penetrant produced by the Magnaflux Corporation was sprayed on the salt surface or applied with a soft tissue paper. Excess dye was immediately wiped off, confining dye penetration to a small depth below the surface. This is necessary to eliminate internal fluorescence from deep cracks which, in the transluscent salt, would mask the fluoresence from the surface.

The samples were then examined with the petrographic microscope using incident ultraviolet light from a portable source.

2.4 Image Analysis

Figures 1 and 2 are photomicrographs of polished and crack-decorated pressed and natural salt. Figure 3 is a tracing of grain boundaries on a surface of natural dome salt. It is readily apparent that the pressed salt grain size is about one order of magnitude finer than that of the natural dome salt. In order to obtain more quantitiative data high contrast prints of the photographs were made on an IBM copying machine and used for image analysis on the Quantimet 900 image analyzer (Cambridge Instruments). The image analyser is equipped with a macro view video camera which scans each photograph,

SC83-21249

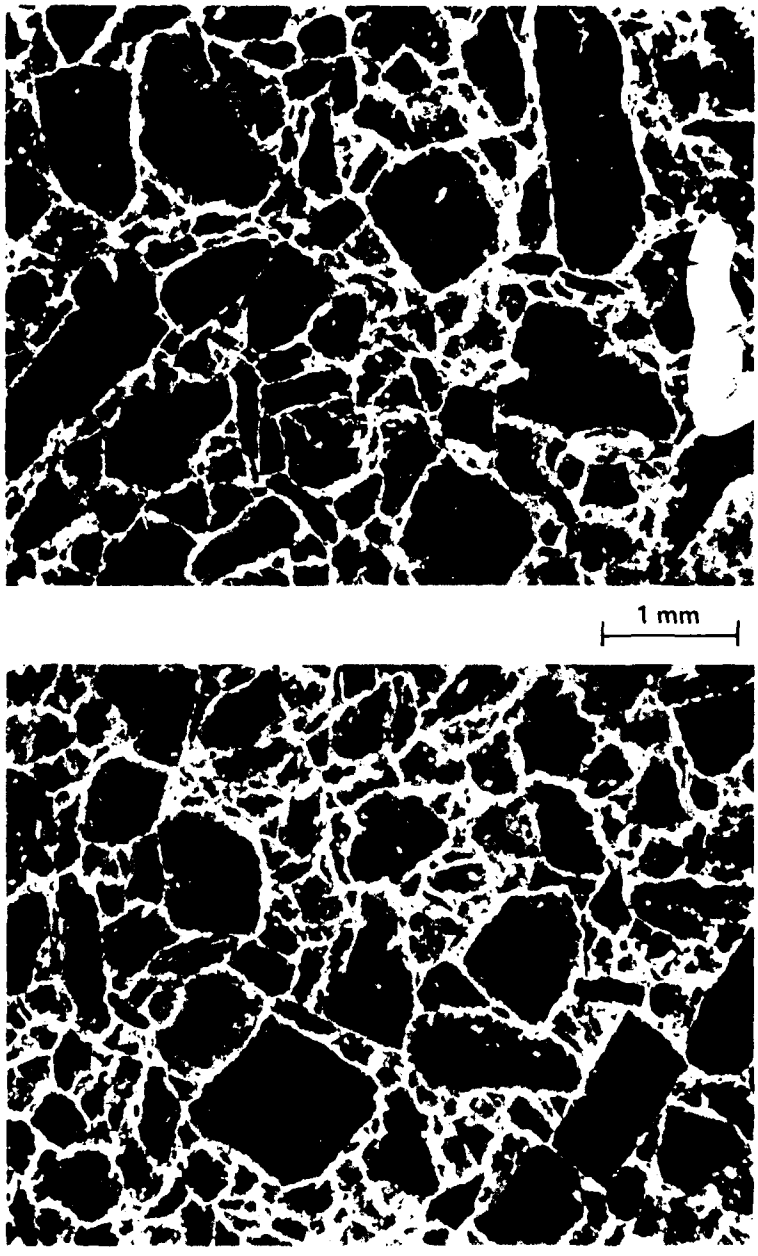

Fig. 1 Photomicrographs of polished and crack-decorated surface of pressed salt.

SC83-21245

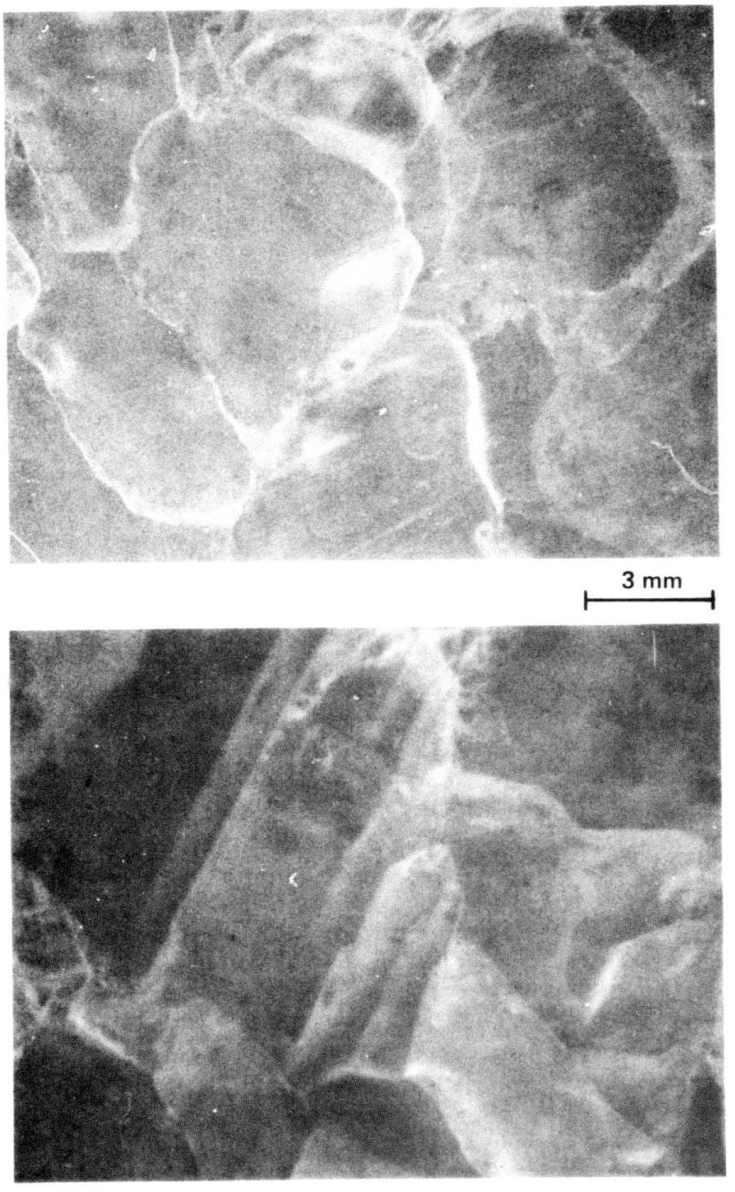

Fig. 2 Photomicrographs of polished and crack-decorated surface of natural dome salt.

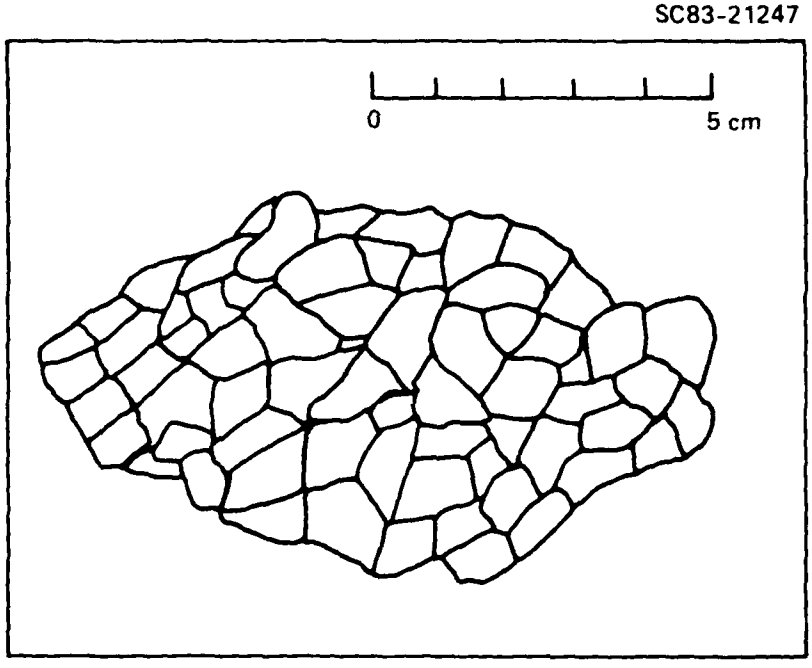

Fig. 3 Tracing of grain boundaries on a surface of natural dome salt.

storing digitized image density values in computer memory. A grain size analysis program was modified to accomodate the grain size range of the pressed salt with the resolution required. The program sorted grains into 23 diameter ranges on a log scale from 10 μm to 2.00 mm. Apparent grain diameter is computed from measured grain surface area, assuming a circular grain.

2.5 Grain Size Distribution

2.5.1 Pressed Salt

Data for pressed salt were obtained by analyzing four photomicrographs, such as those illustrated in Fig. 1. The grain count versus grain diameter values are given in Table 1. Measurements were limited to grain sizes between 35 μm and 2257 μm in diameter.

The number of grain counts per diameter range (Table 1) were computed from grain area measurements, assuming a circular shape. The data represent apparent grain size values measured on a random cross-section, and do not represent true grain size values. This is illustrated in Fig. 4 where spheres of a given grain size generally appear in cross-section to be smaller than in reality. A computer program was written to make appropriate corrections based on the methods developed by Johnson (1946), Saltikov (1958) and more recently discussed by Underwood (1968).

Corrected values for grain size distribution by volume percent and grain count percent are given in Table 2. Figure 5 is a histogram of the volume percent versus grain size values.

These results are for one surface of pressed salt. Assuming reasonable homogeneity the general shape of the histogram should be representative of the pressed salt material. Most of the pressed salt grains were less than 100 μm in diameter. However, the population was dominated volumetrically by a small number of grains greater than 500 μm in diameter. Microscopic examination suggests that in the process of pressing the salt many large grains were crushed to fill the intergranular spaces. Thus the grain size distribution

Table 1

Raw Apparent Grain Size Data for Pressed Salt Showing the Number of Grains Measured in Each Increment of Log Apparent Diameter

Grain Size Analysis of Pressed Salt (Uncorrected Data)	
Log Apparent Diameter (μm)	Counts
3.2 - 3.3	0
3.1 - 3.2	3
3.0 - 3.1	2
2.9 - 3.0	6
2.8 - 2.9	10
2.7 - 2.8	16
2.6 - 2.7	17
2.5 - 2.6	25
2.4 - 2.5	28
2.3 - 2.4	21
2.4 - 2.3	33
2.1 - 2.2	34
2.0 - 2.1	39
1.9 - 2.0	51
1.9 - 1.9	33
1.7 - 1.8	44
1.6 - 1.7	43
1.5 - 1.6	24

SC83-21246

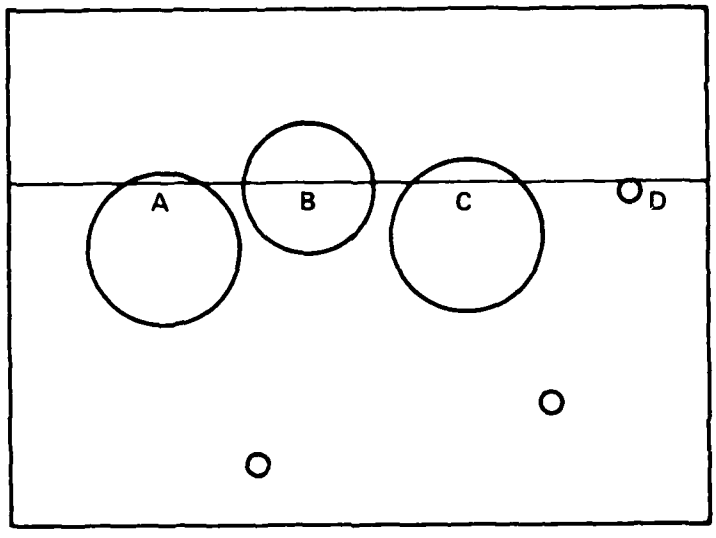

Fig. 4 Schematic illustration of a random cut through a spacial distribution of spheres. Apparent grain diameters in cross section will generally be less than actual diameters (A and C); grains with different diameters (B and C) may appear identical.

Table 2

Corrected Grain Size Data for Pressed Salt Showing the Percentage of Grains, Expressed in Terms of Volume and Grain Count, in Each Increment of Log Diameter

Grain Size Analysis of Pressed Salt (Corrected Data)*		
Log Diameter (μm)	Vol. %	Grain Count (%)
3.2 - 3.3	0.000	0.000
3.1 - 3.3	20.679	0.087
3.0 - 3.1	5.988	0.050
2.9 - 3.0	14.419	0.242
2.8 - 2.9	14.444	0.485
2.7 - 2.8	14.223	0.952
2.6 - 2.7	8.304	1.109
2.5 - 2.6	8.154	2.173
2.4 - 2.5	5.306	2.821
2.3 - 2.4	1.797	1.906
2.2 - 2.3	2.481	5.252
2.1 - 2.2	1.469	6.205
2.0 - 2.1	1.080	9.097
1.9 - 2.0	0.958	16.115
1.8 - 1.9	0.231	7.762
1.7 - 1.8	0.286	19.125
1.6 - 1.7	0.163	21.813
1.5 - 1.6	0.018	4.806

*Corrected according to Johnson-Saltykov Procedure (Underwood, 1968).

SC83-21248

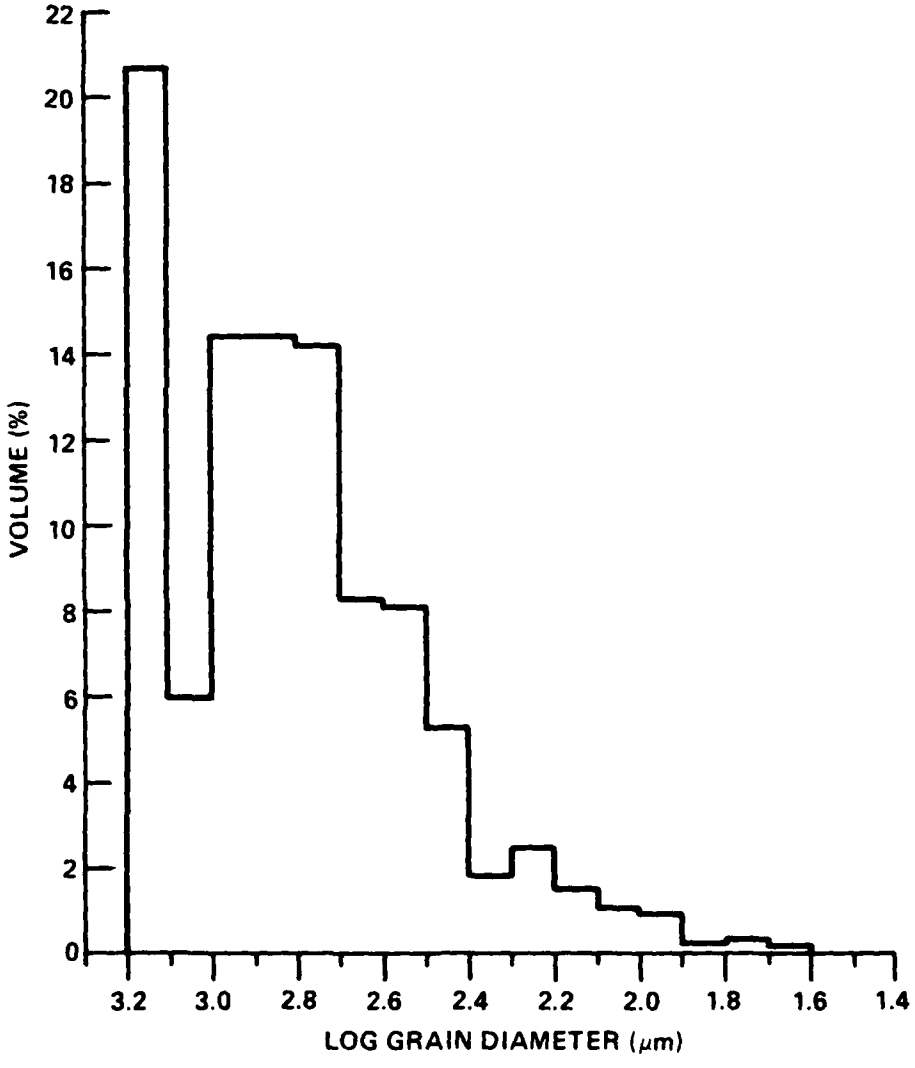

Fig. 5 Histogram showing the volume percent of grains in each increment of log grain diameter.

shown here does not distinguish between grain contacts of the original grains and those caused by grain fracture. All the surfaces penetrated by the fluorescent dye are thus assumed to be cracks between individual grains.

2.5.2 Natural Salt

Image analysis of natural salt surfaces was not performed during this period because a large surface is required for a measuring statistically meaningful number of grains. Techniques for imaging large surfaces will be developed during a follow-on study. It is, however, apparent that grains in the natural salt are an order of magnitude larger than grains in the pressed salt. Furthermore, the dome salt shows macroscopic flow structures and preferred crystal orientation that will be investigated quantitatively in more detail.

3.0 EXPERIMENTAL METHODS

3.1 Experimental Apparatus

Two different types of resonant bar apparatus have been used to measure the energy dissipation factor, Q^{-1}, in both pressed salt and natural dome salt. In both cases, Q^{-1} is obtained by dividing the power half-width of the swept resonance curve (i.e., the bandwidth measured at $1/\sqrt{2}$ maximum peak height) by the resonant frequency. A pair of electromagnetic transducers is used in both types of apparatus. A block diagram of instrumentation used in swept resonance measurements is shown in Fig. 6. The oscillation frequency of the driving transducer is swept slowly across the resonance peak, and the signal induced by vibration into the receiving transducer is monitored simultaneously. Plots of transducer output vs frequency are made using an x-y recorder. The sensitivity of the receiving transducer can be calibrated using a capacitive microphone, enabling a calculation of maximum strain amplitude for the specimen from measurements of peak height, amplifier gain, and specimen dimensions. The maximum strain amplitude for vibrations in torsion and flexure is defined in Figs. 7 and 8, respectively.

In the first type of apparatus, a cylindrical specimen (typically 1.42 cm diam. by 15 cm long) is held at the center, which is a position of zero axial motion for fundamental axially symmetric vibrations in torsion and extension. A small ferromagnetic tab is cemented to each specimen end. One of these tabs couples magnetically to the oscillating field around one electromagnetic transducer and is used to excite the sample vibration. The tab on the opposite end induces current into a second electromagnetic transducer and is used to monitor vibration amplitude. Using this type of apparatus with the specimen held in the center inertial loading is very small and resonant frequencies are typically in the range of 12 kHz for salt in extension.

Tittmann and Curnow (1976) describe the second type of apparatus (Fig. 9), which enables the addition of massive inertial rotors to each end of the specimen, resulting in much lower characteristic frequencies. Resonant

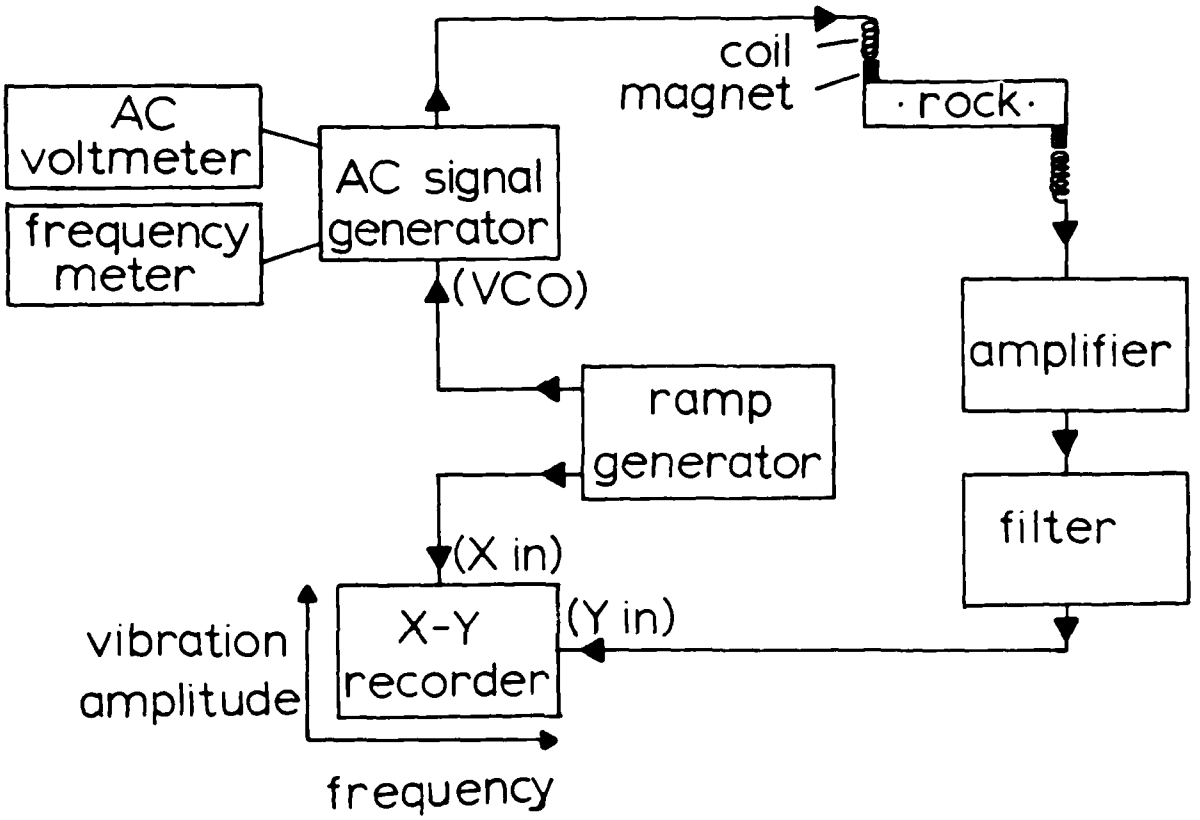

Fig. 6 Schematic block diagram of instrumentation used to measure attenuation by the swept resonance technique.

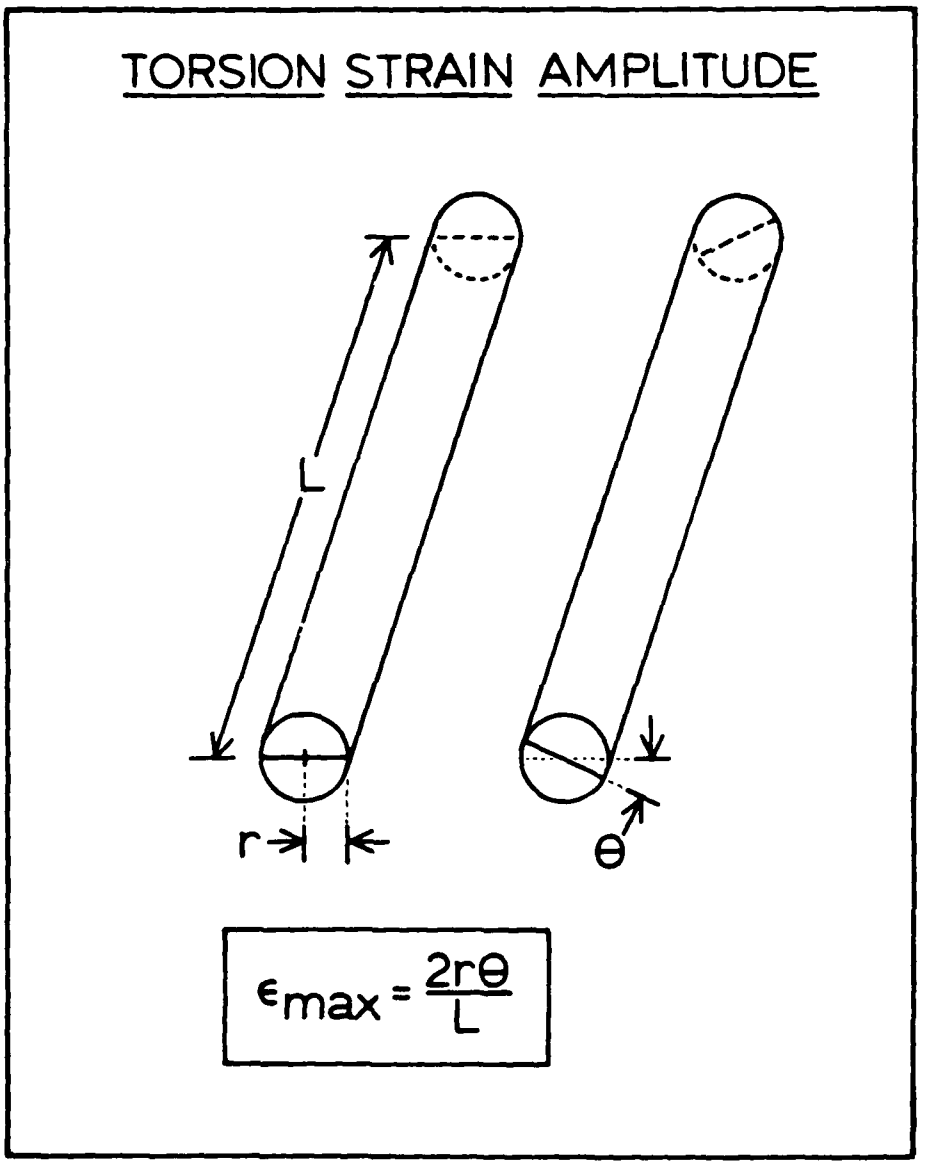

Fig. 7 Definition of vibration strain amplitude in torsion.

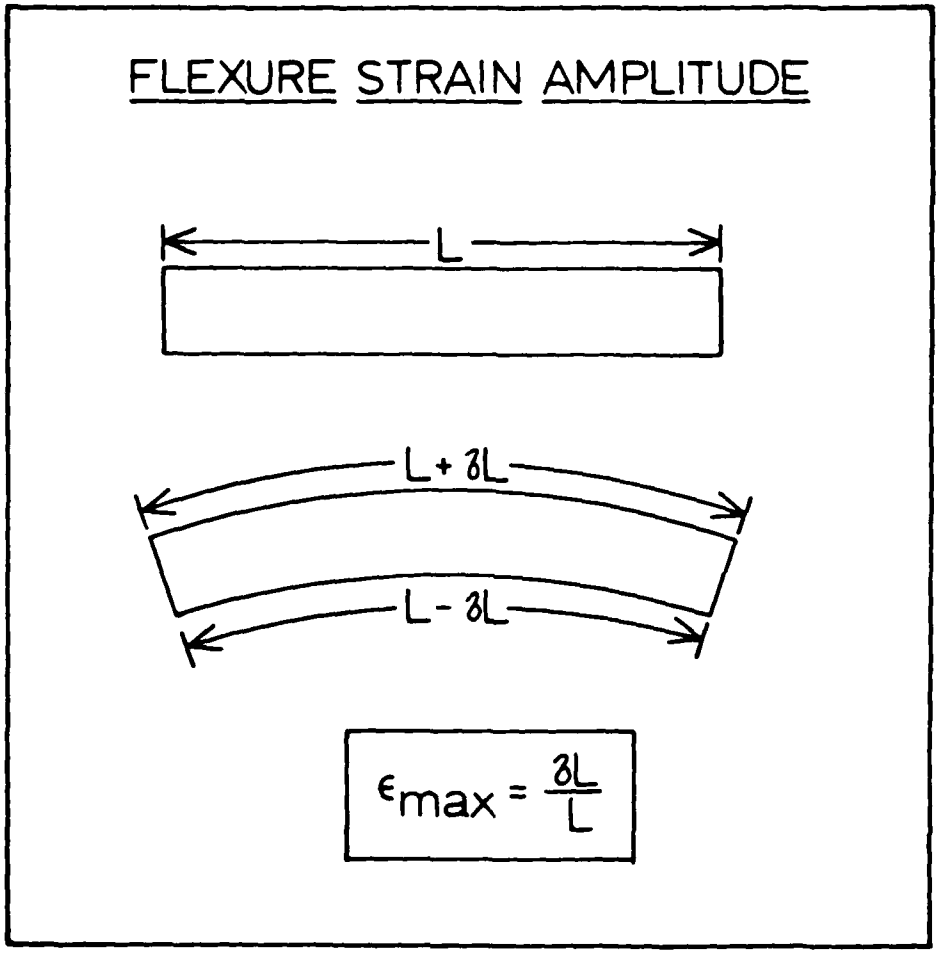

Fig. 8 Definition of vibration strain amplitude in flexure.

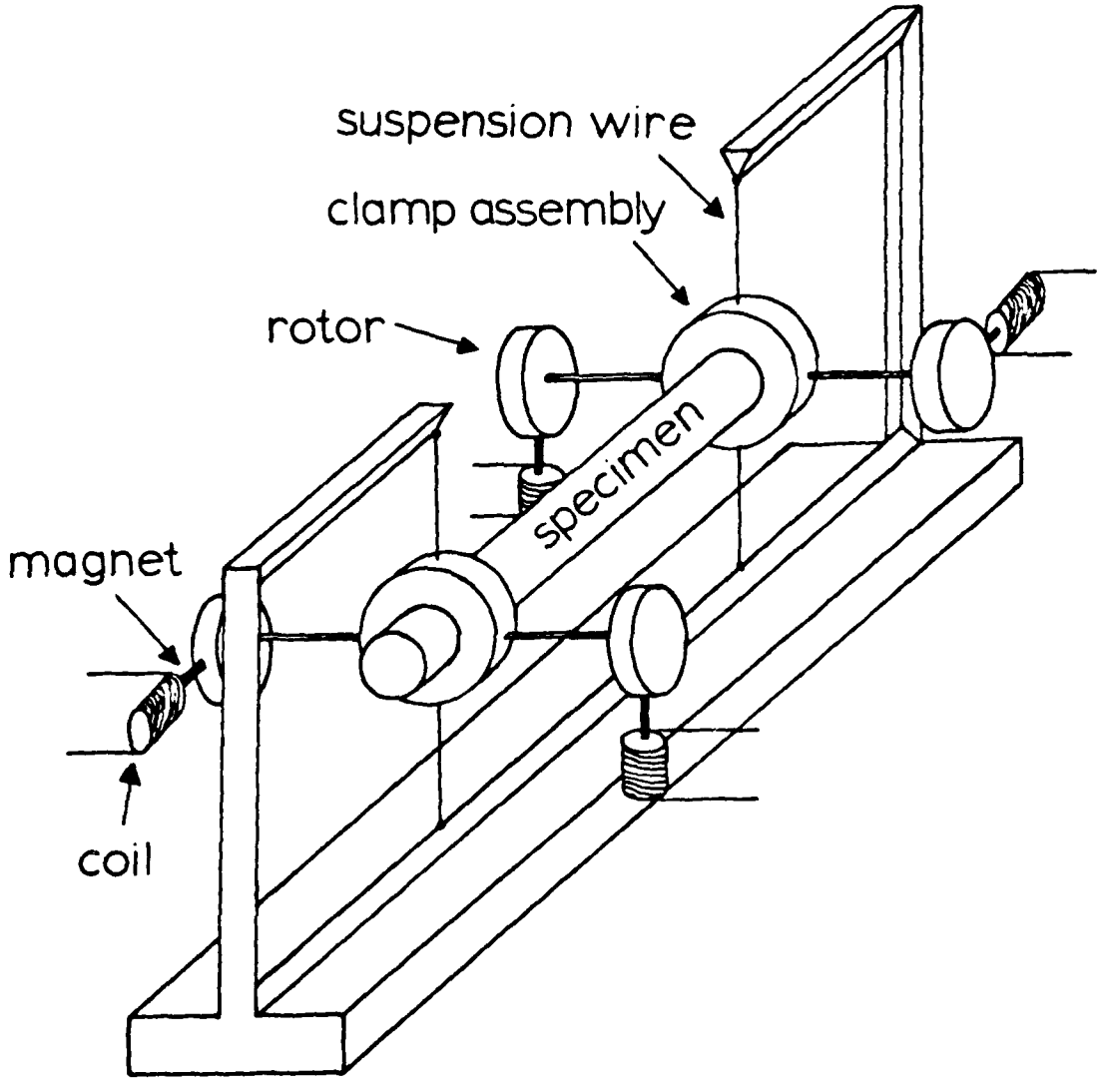

Fig. 9 Schematic illustration of resonant bar apparatus used for measurements between 50 Hz and 470 Hz.

vibrations are driven in either torsion or flexure using electromagnetic transducers. Reliable data have been obtained for both pressed salt and dome salt at frequencies from ~ 50 Hz to ~ 400 Hz.

3.2 Testing Procedures

During the first half of the contract period, studies were concentrated on polycrystalline salt which was pressed at 120°C and 0.14 GPa for 1 hour. Two cylinders of this material, each approximately 40 cm long and 40 cm diameter were obtained from Donald Larson at Lawrence Livermore Laboratory, and are presumed to be identical to the material used by Larson in his studies of near-field particle motion associated with small laboratory scale explosions in salt (Larson, 1981). During the latter part of the contract period, the behavior of natural dome salt was also investigated. Test specimens of natural dome salt were cut from a large block (approx. .51 × .66 × 1.65m) obtained from the Kleer Salt Mine operated by the Morton Salt Co. in the Grand Saline salt dome in eastern Texas. Cylindrical test specimens 1.42 cm in diameter were cut from these blocks using a gas-cooled diamond coring machine. Cores were trimmed to approximately 12-16 cm finished length.

Under any given set of conditions, both resonant frequency and the RMS voltage applied to the driving transducer were measured. Measurements on pressed salt were obtained at various vibration amplitudes. Corresponding values for strain amplitude and Q^{-1} were calculated at several different frequencies between 50 Hz and 12 kHz, and at different levels of humidity (25%, 35%, 50%) under ambient pressure condtions. In addition, one pressed salt specimen was jacketed in a mylar tube 0.076 mm thick and studied in flexure at ~ 470 Hz. The behavior of natural dome salt was studied at elevated pressures. Measurements were made in torsion and flexure at several effective pressures up to 6.8×10^7 Pa and at several frequencies from 80 to 480 Hz.

3.3 Experimental Evidence for Linear and Nonlinear Behavior

Three different approaches have been used to evaluate the degree to which the material being tested behaves linearly. The first involves examining the graphs of log input voltage (i.e., the voltage applied to the excitation transducer) plotted against log strain amplitude, which is directly proportional to the voltage output of the transducer monitoring the sample vibration. In the second approach, the resonant frequency is examined as a function of vibration strain amplitude, and in the third, changes in the attenuation factor, Q^{-1}, with vibration amplitude reflect nonlinearity. Each of these methods is discussed below.

3.3.1 Input Voltage vs Strain Amplitude

Attenuation in a resonant system can be obtained from an analysis of excitation force and displacement. The following analysis is taken from Harbottle (1970).

The force, F, exerted on the specimen by the driving coil is given by $F = F_0 \sin \theta$. At resonance the displacement, X, is given by $X = X_0 \cos \theta$ and the work done in one cycle, ΔE, is given by

$$\Delta E = - \int F dX$$

$$= -2 F_0 X_0 \int_0^{\pi} \sin^2 \theta \, d\theta$$

$$= -\pi F_0 X_0 \quad .$$

Assuming that F_0 is related to the RMS voltage, V_0, applied to the driving coil by $F_0 = aV_0$ and that the total energy of oscillation is given by $E = bX_0^2$ where a and b are constants, then

$$Q^{-1} = \frac{\Delta E}{2\pi E} = C \frac{V_0}{X_0}$$

where C is constant. Therefore, a plot of log excitation voltage vs log strain amplitude should result in a straight line with unity slope over the range of constant Q (linear) behavior.

3.3.2 Resonant Frequency vs Log strain Amplitude

A necessary condition for linear behavior is that the elastic modulus be independent of the level of stress on the specimen. Therefore, if the resonant frequency changes with vibration amplitude, reflecting changes in modulus, it would indicate a violation of the linearity condition.

3.3.3 Attenuation vs Log Strain Amplitude

A plot of attenuation against log strain amplitude is the most sensitive method for revealing small amounts of nonlinear behavior. If the system behaves linearly, attenuation, which is proportional to the fraction of energy dissipated per cycle, should be independent of strain amplitude. However, an increase in attenuation with increasing strain amplitude would necessarily indicate an increase in the amount of relaxation with an associated decrease in modulus. Very small modulus decreases would not necessariy be reflected as a significnat decrease in resonant frequency, particularly at low frequencies. Thus, attenuation measurements can be used as a very sensitive indicator of nonlinear behavior in that they reflect directly to the degree to which the system deviates from linearity rather than the degree to which the system obeys linearity.

4.0 EXPERIMENTAL RESULTS

4.1 Pressed Salt

4.1.1 Analysis of Nonlinear Behavior

The data plotted in Figs. 10 and 11 for pressed salt in flexure at ~ 413 Hz and 55% humidity are typical of most pressed salt measurements. In Fig. 10, input voltage (V_{in}) and resonant frequency are plotted against the log of the maximum strain amplitude. Both the drop in resonant frequency and the deviation from unity slope in the V_{in}-log strain amplitude data at strain amplitudes greater than 2×10^{-6} are indicative of obvious nonlinear effects at high strain amplitudes. An examination of the attenuation data in Fig. 11, however, indicates that weak nonlinear effects persist at low strain amplitudes, at least lown to 10^{-8}. Thus, two regimes are clarly defined. The system is strongly nonlinear at strain amplitudes greater than 2×10^{-6} and weakly nonlinear at lower strain amplitudes. Totally linear behavior was not observed in pressed salt under any of the conditions studied as will be shown.

4.1.2 Effects of Frequency on Attenuation at Ambient Pressure and 35% Relative Humidity

Measurements of attenuation as a function of strain amplitude at several different frequencies in torsion and flexure are presented in Figs. 12 and 13, respectively. The transition from the domain of weak nonlinearity to strong nonlinearity occurs at a strain amplitude of about 2×10^{-6} in all cases. However, at any given amplitude and level of atmospheric humidity, total attenuation decreases with increasing frequency, implying a slow characteristic relaxation time.

4.1.3 Effects of Humidity on Attenuation Under Ambient Pressure Conditions

The data presented in Figs. 14, 15 and 16 show the effects of atmospheric humidity on the attenuation in pressed salt. Once again, the transition

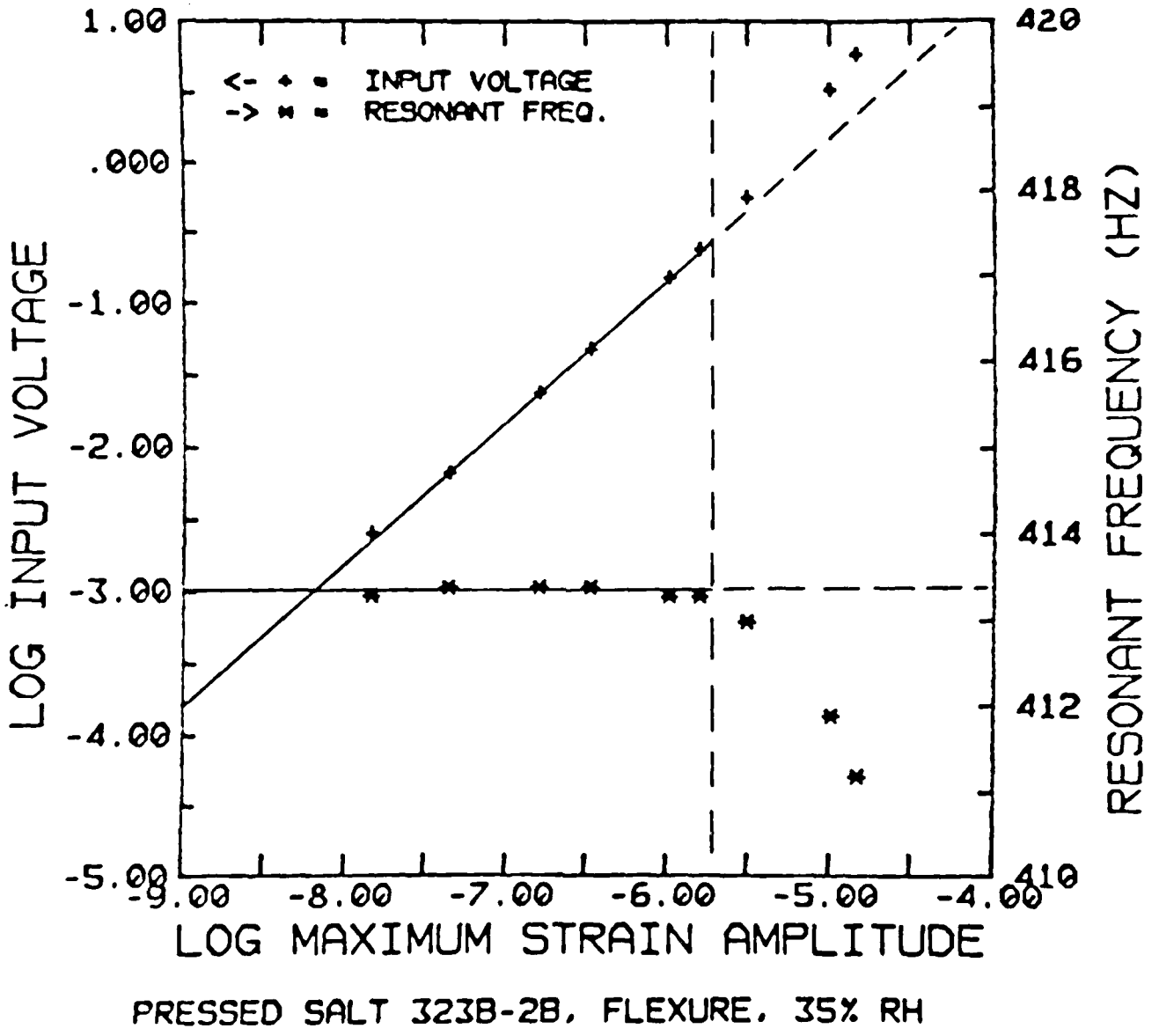

Fig. 10 Log input voltage and resonant frequency plotted against log maximum vibration amplitude for pressed salt flexure at 35% relative humidity.

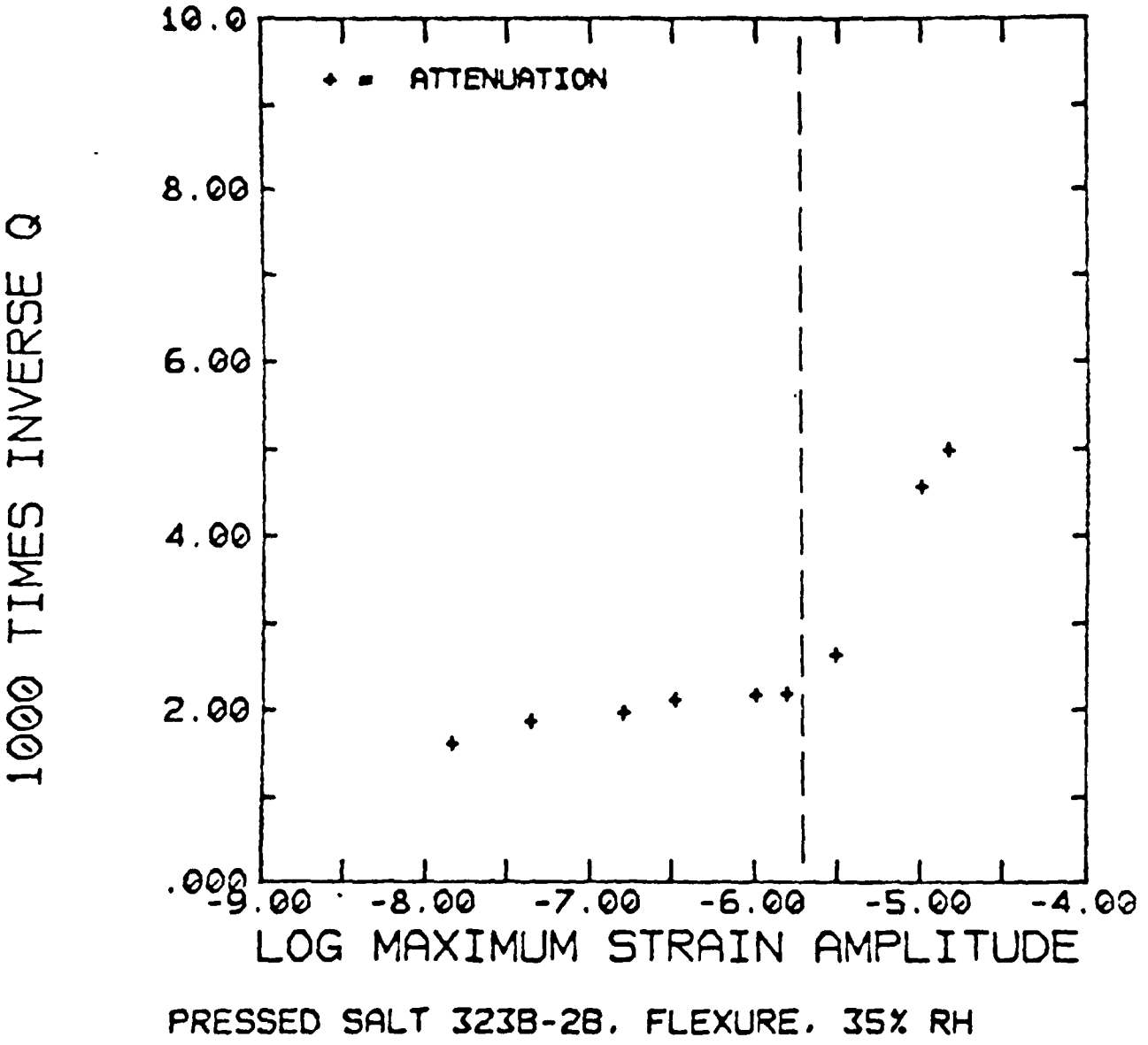

Fig. 11 Attenuation plotted against log maximum vibration amplitude for pressed salt in flexure at 35% humidity and 413 Hz.

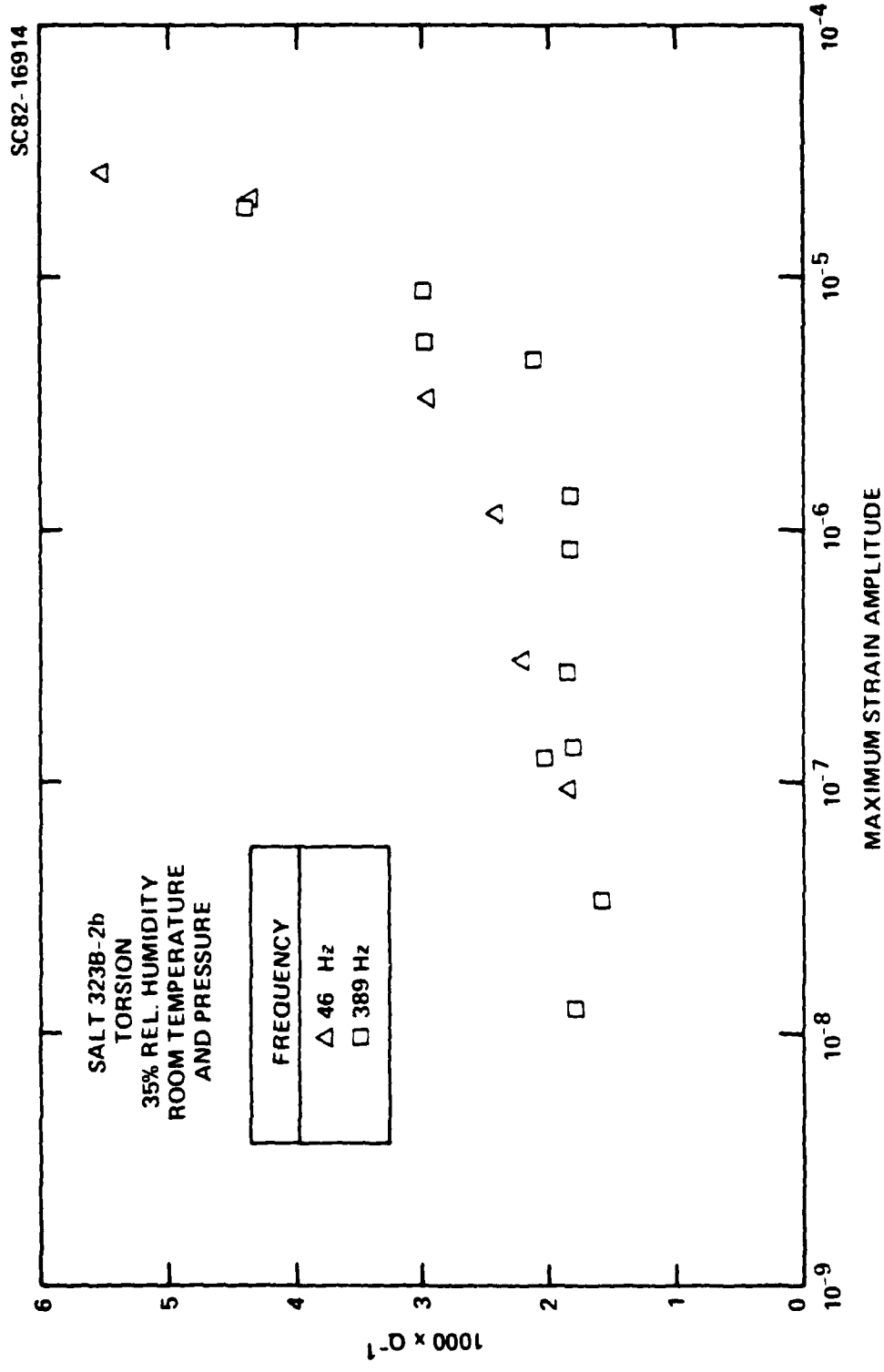

Fig. 12 Attenuation plotted against log maximum vibration amplitude for pressed slat in torsion at 35% humidity and at two different frequencies.

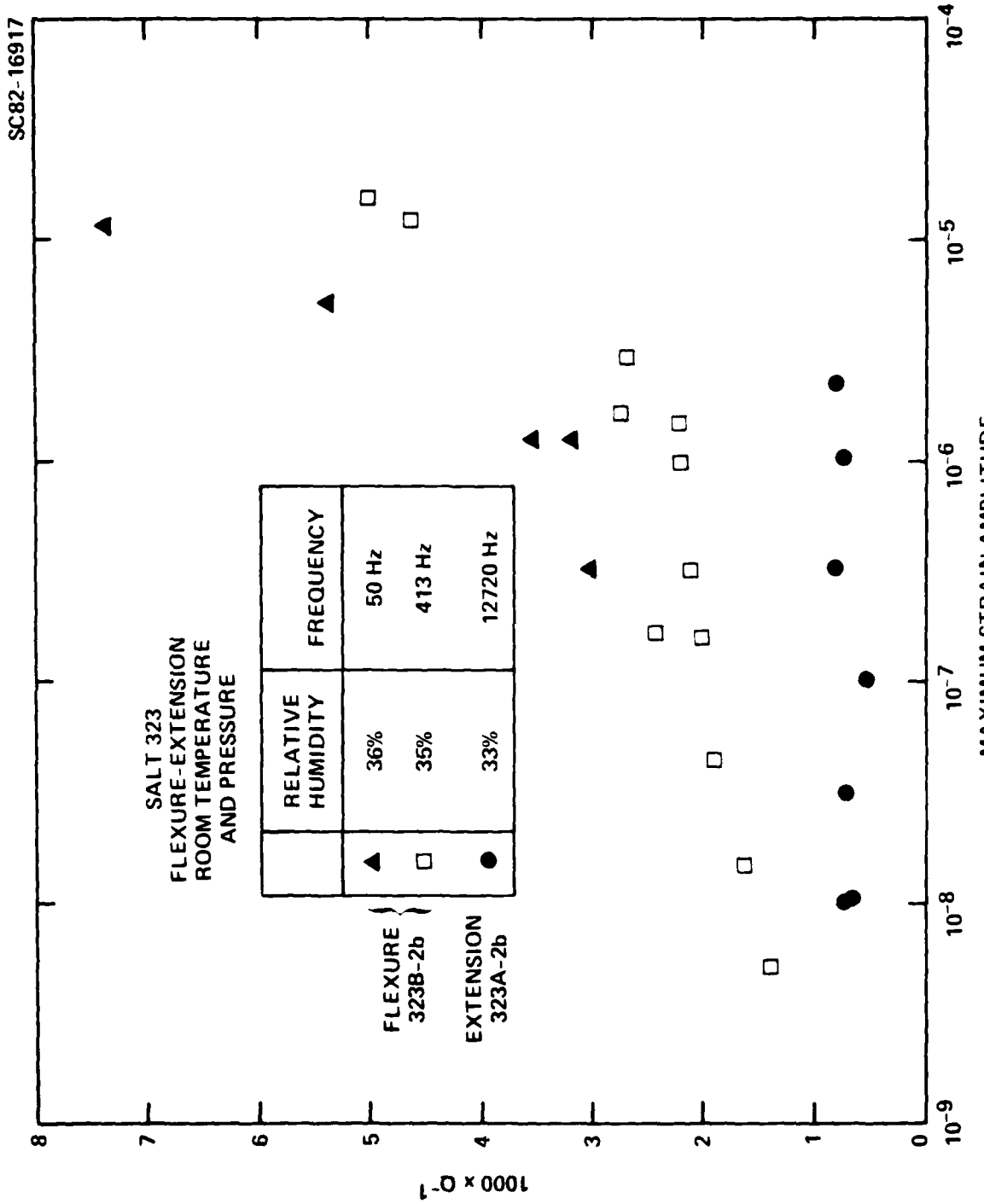

Fig. 13 Attenuation plotted against log maximum vibration amplitude for pressed salt in flexure/extension at 35% humidity and at three different frequencies.

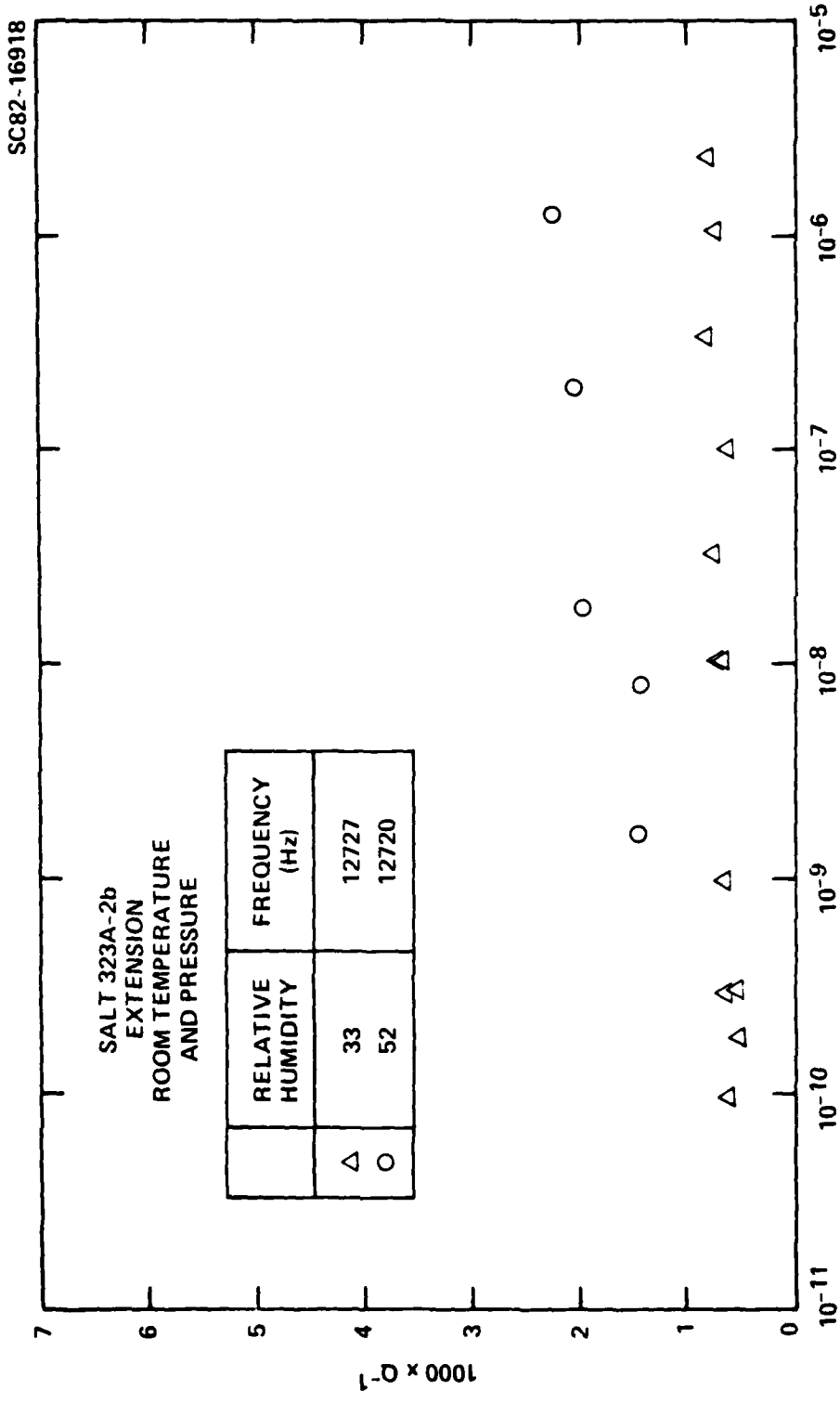

Fig. 14 Attenuation plotted against log maximum vibration amplitude for pressed salt in extension at 12.7 kHz and at two different levels of ambient humidity.

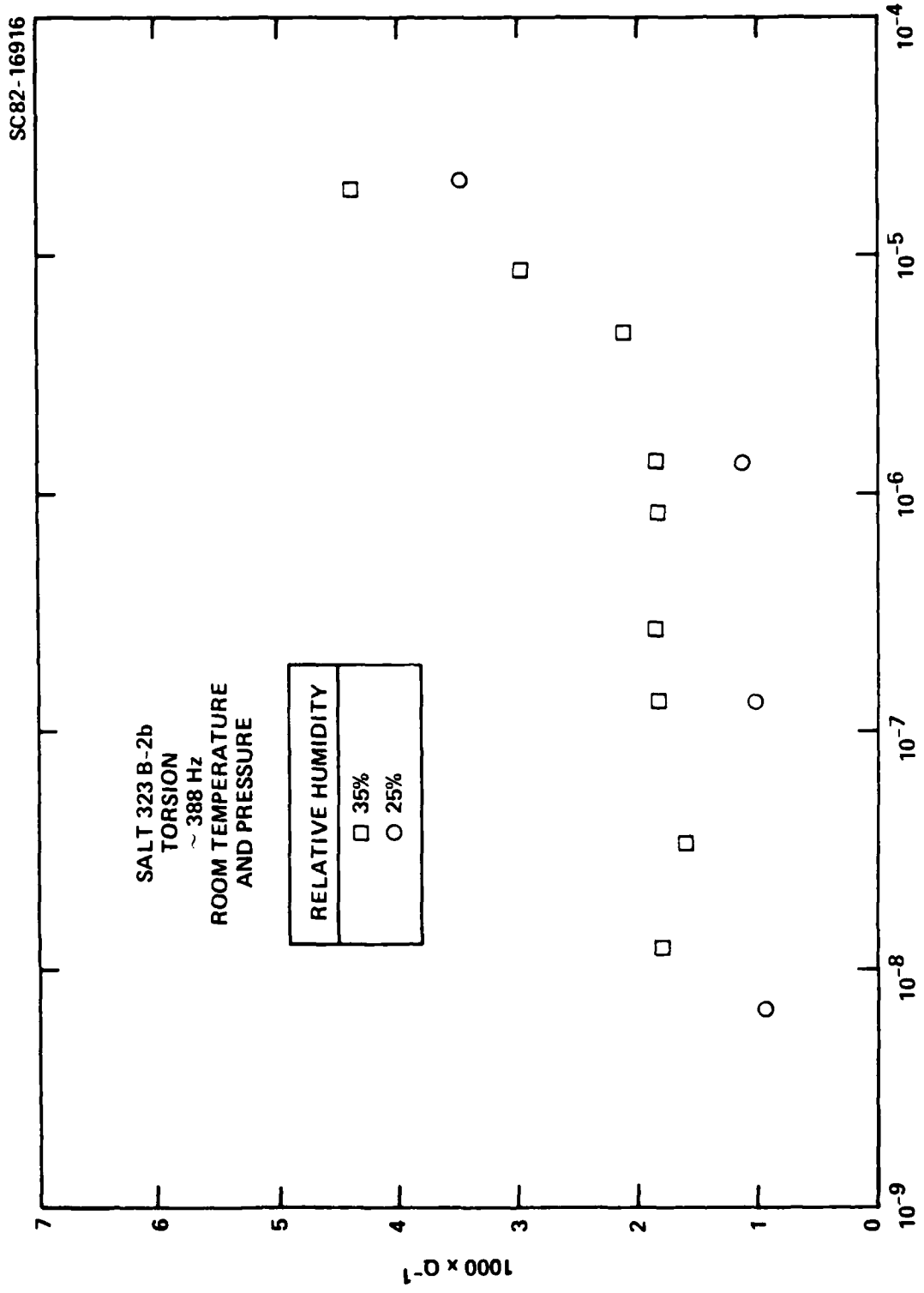

Fig. 15 Attenuation plotted against log maximum vibration amplitude for pressed salt in torsion at 388 Hz and at two different levels of humidity.

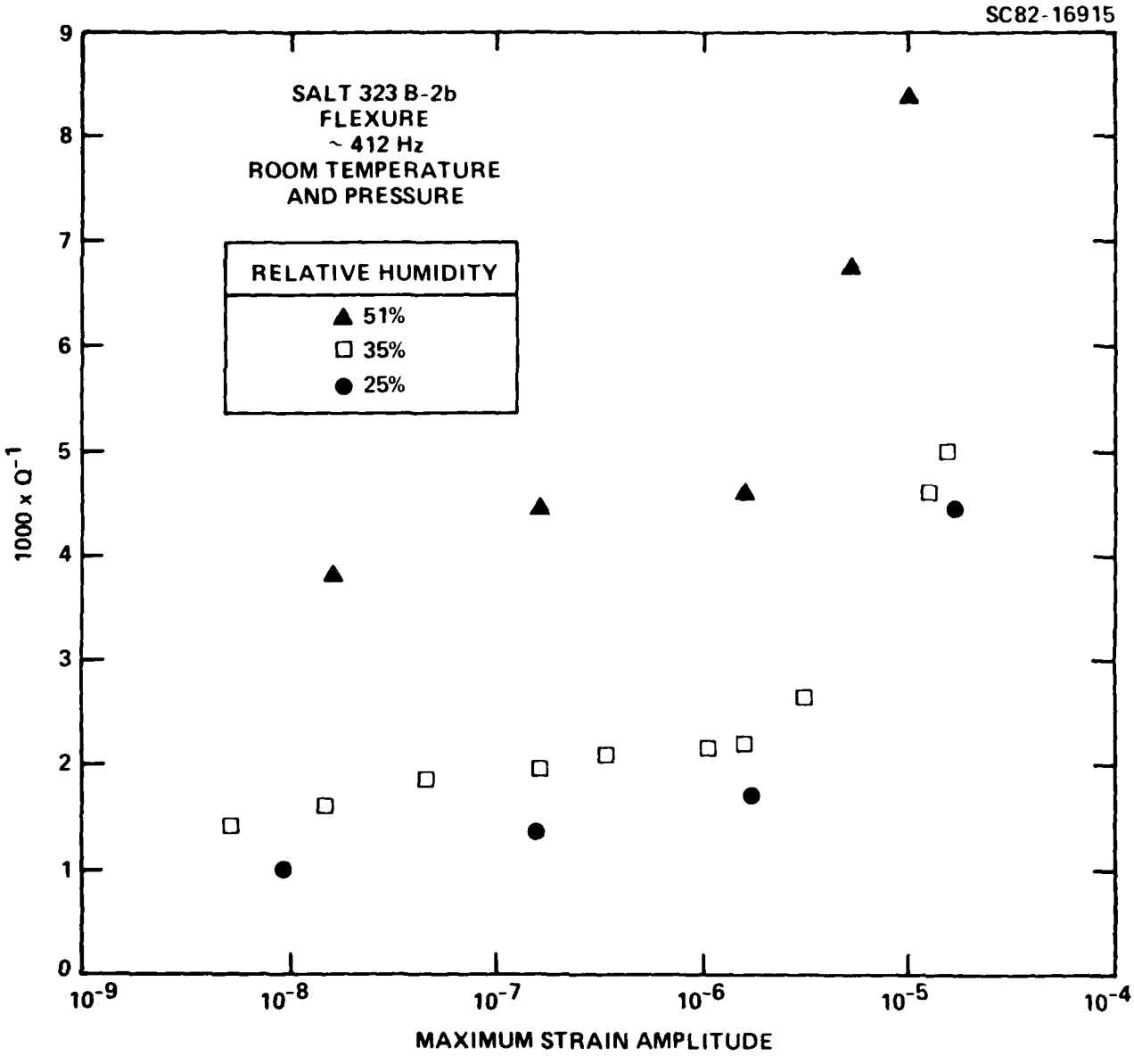

Fig. 16 Attenuation plotted against log maximum vibration amplitude for pressed salt in flexure at 412 Hz and at three different levels of ambient humidity.

from weak to strong nonlinearity occurs at about 2×10^{-6} strain amplitude. At any given frequency and level of maximum strain amplitude, attenuation increases with increasing humidity.

4.1.4 Attenuation at Elevated Effective Pressures

Figure 17 shows attenuation plotted against strain amplitude at several different pressures for pressed salt in flexure at about 470 Hz. The numbers in parenthesis indicate the sequence in which the measurements were made. The first set of measurements at 0 Pa shows strong nonlinear behavior at rather low levels of strain amplitude (3.2×10^{-8}). It is felt that this strong nonlinearity is an indication of some microstructural damage due to high stresses on the sample during preparation and loading. During the ambient pressure experiments, it was found that the dissipation factor Q^{-1} decreased with time after the system was mechanically adjusted, and that it stabilized after about 12 hours. Stress-induced microcracks probably healed during this time, a process which was catalized by adsorbed moisture. In the high pressure experiment, the same process of crack healing was accomplished by combined time and pressure.

The following observations are significant: a) even at effective pressures of 1.24×10^{8} Pa, weakly nonlinear behavior is observed between maximum strain amplitudes of 3.2×10^{-8} and 3.2×10^{-5}; b) the transition to strongly nonlinear behavior at high strain amplitudes was not observed at effective pressures greater than or equal to 1.38×10^{7} Pa, even at strain amplitudes near 3×10^{-5}.

4.2 Natural Dome Salt

A specimen of natural dome salt was studied at elevated effective pressures up to 6.8×10^{7} Pa. Three different experimental measurements were obtained as a function of vibration amplitude in order to test for linear versus nonlinear behavior using the resonant bar apparatus. In the domain of linear behavior, attenuation and resonant frequency are expected to be

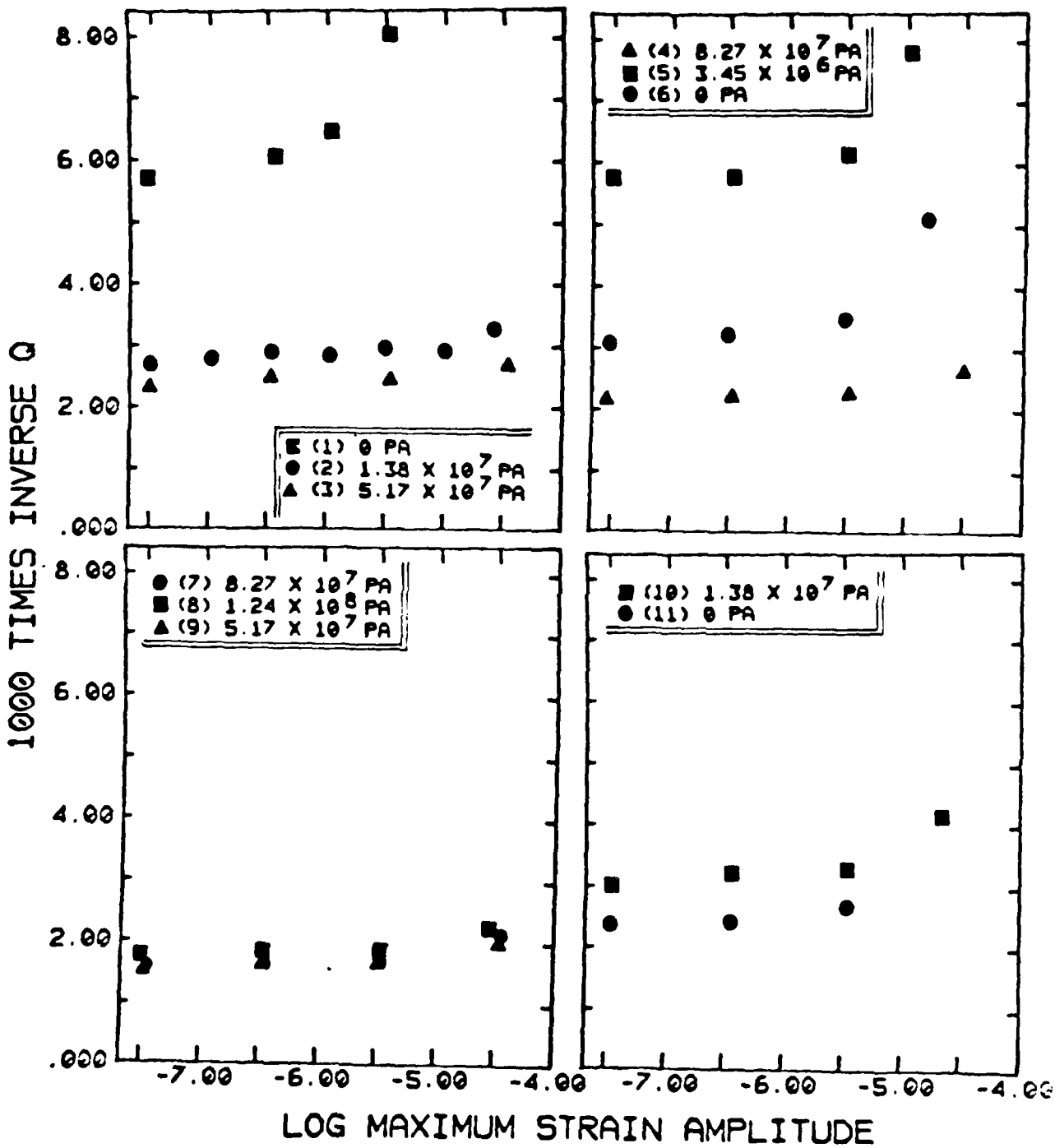

Fig. 17 Attenuation plotted against log maximum vibration amplitude for pressed salt at 470 Hz and at several different effective pressures. Pressure was cycled several times, with the numbers in parenthesis representing the sequence of measurement.

independent of vibration amplitude, and the driving voltage is expected to vary linearly with vibration amplitude. In Figs. 18-23, attenuation, resonant frequency and log driving voltage are plotted as a function of log maximum vibration amplitude. Figure 18 shows measurements taken in flexure at a number of different effective pressures. Pressure was cycled in the order 1-6. Figure 19 shows the corresponding data taken in torsion. The following observations are significant: (1) the threshold amplitude for nonlinear behavior occurs near 10^{-6} at high effective pressures, or after the sample has effectively been cold-pressed at elevated effective pressures (contrast (5) with (2)). (2) Linear anelastic attenuation is higher for extensional waves (flexure) than for shear waves, (3) Q is nearly independent of pressure in the linear regime, (4) at very low effective pressures, nonlinear effects persist in the lowest amplitude measurements (10^{-8}).

Figures 20-23 show the effects of changing frequency at two different effective pressures in both torsion and flexure. The following observations can be drawn from these figures: (1) attenuation for longitudinal waves (flexure) appears to be mildly frequency-dependent in the linear regime, whereas attenuation for shear waves in the linear regime appears to be independent of frequency, and (2) the threshold amplitude for nonlinear behavior (near 10^{-6}) does not vary significantly with frequency.

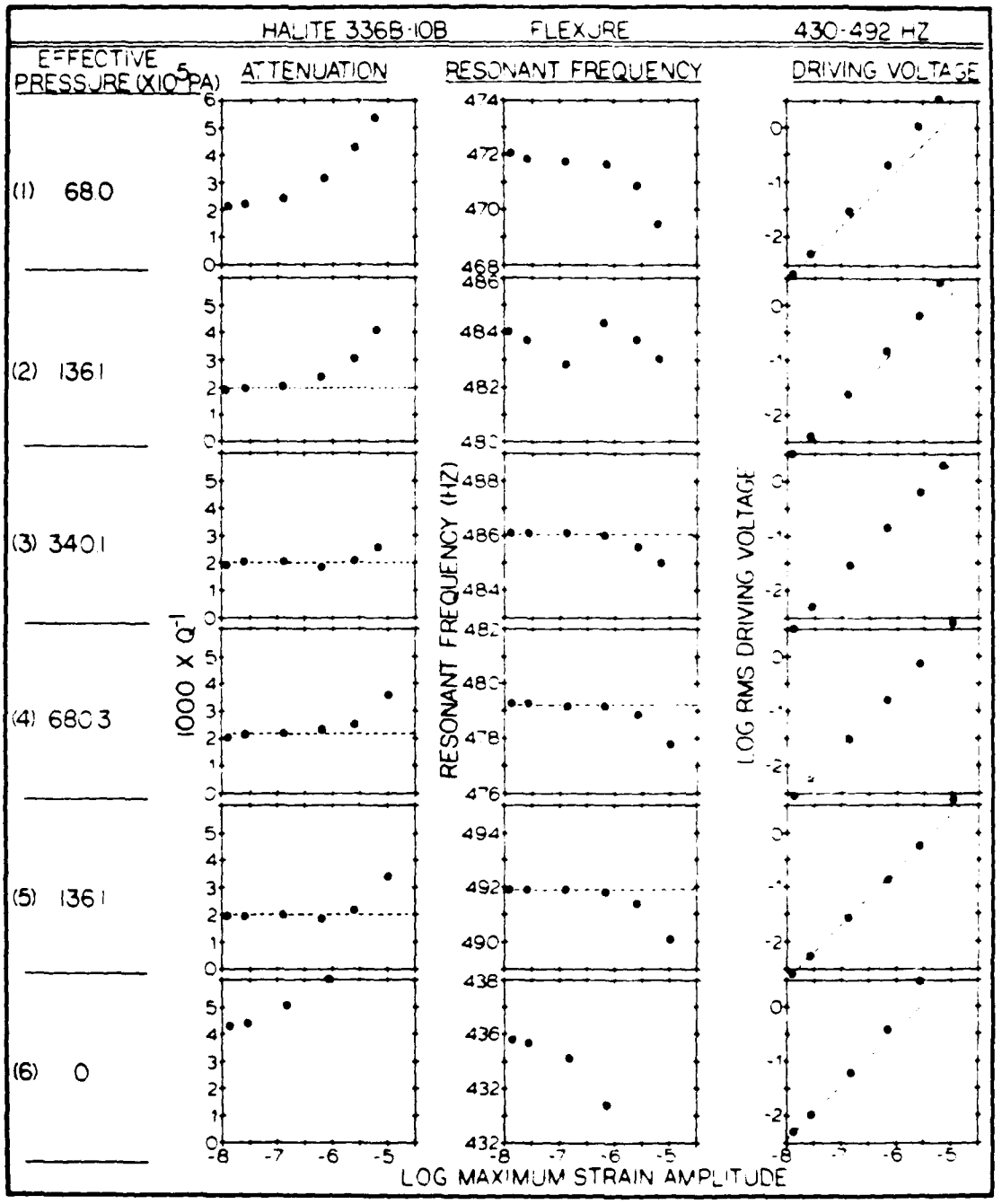

Fig. 18 Attenuation, resonant frequency, and log driving voltage plotted as a function of log maximum vibration amplitude for extensional waves (flexure) at 430-492 Hz, and at several effective pressures up to 6.8×10^7 Pa.

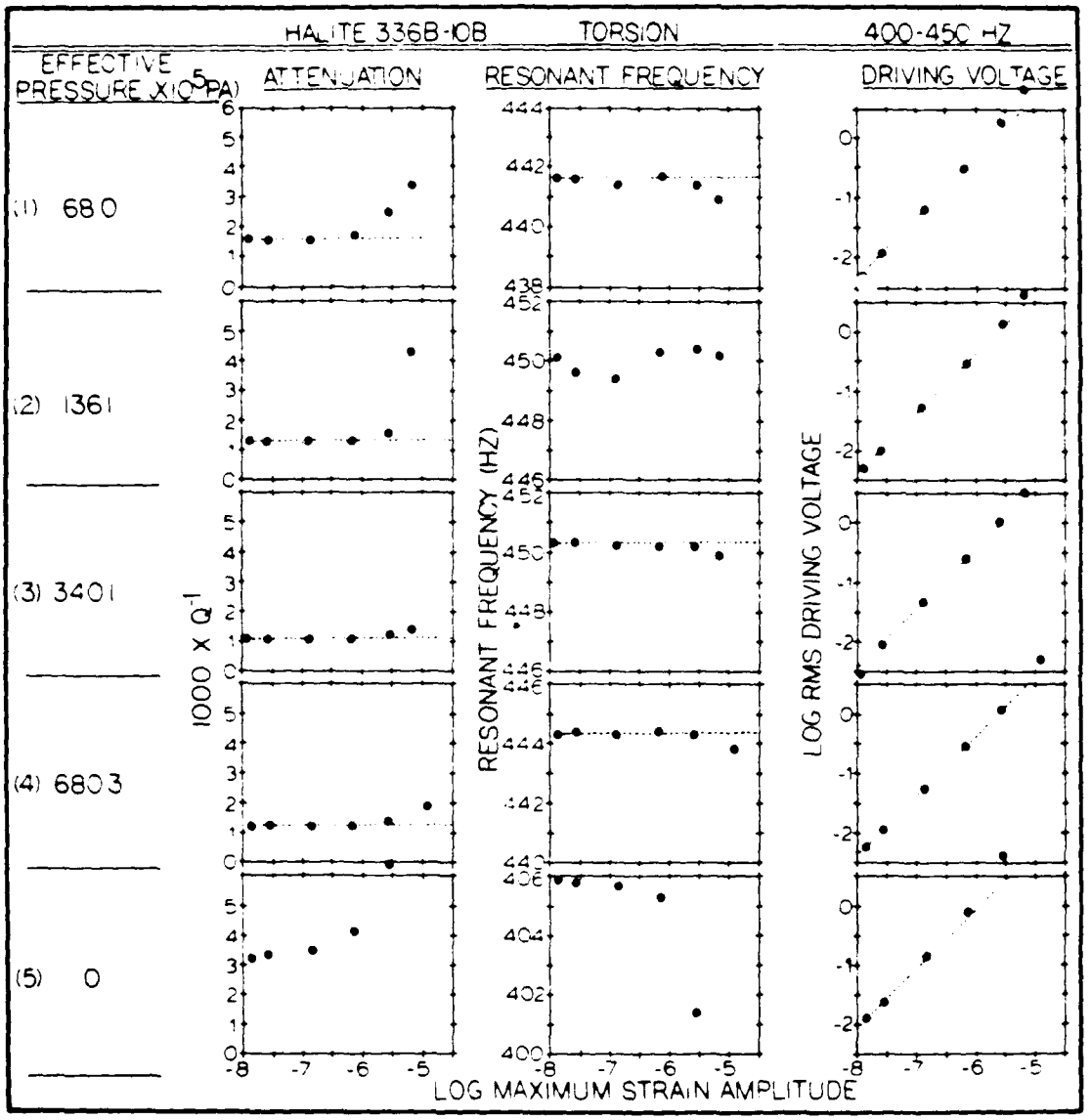

Fig. 19 Attenuation, resonant frequency, and log driving voltage plotted as a function of log maximum vibration amplitude for shear waves (torsion) at 400-450 Hz, and at several effective pressures up to 6.8×10^7 Pa.

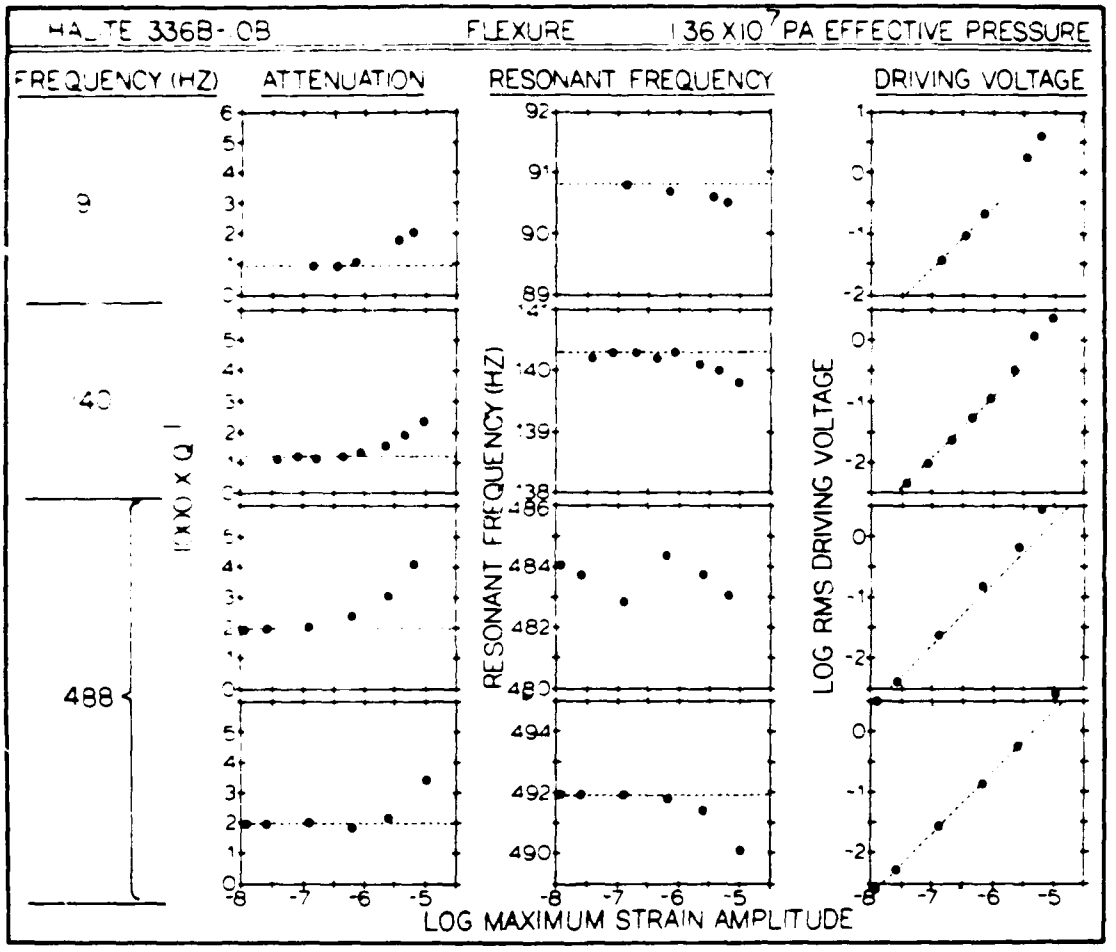

Fig. 20 Attenuation, resonant frequency, and log driving voltage plotted as a function of log maximum vibration amplitude for extensional waves (flexure) at 1.36×10^7 Pa effective pressure, and at several frequencies.

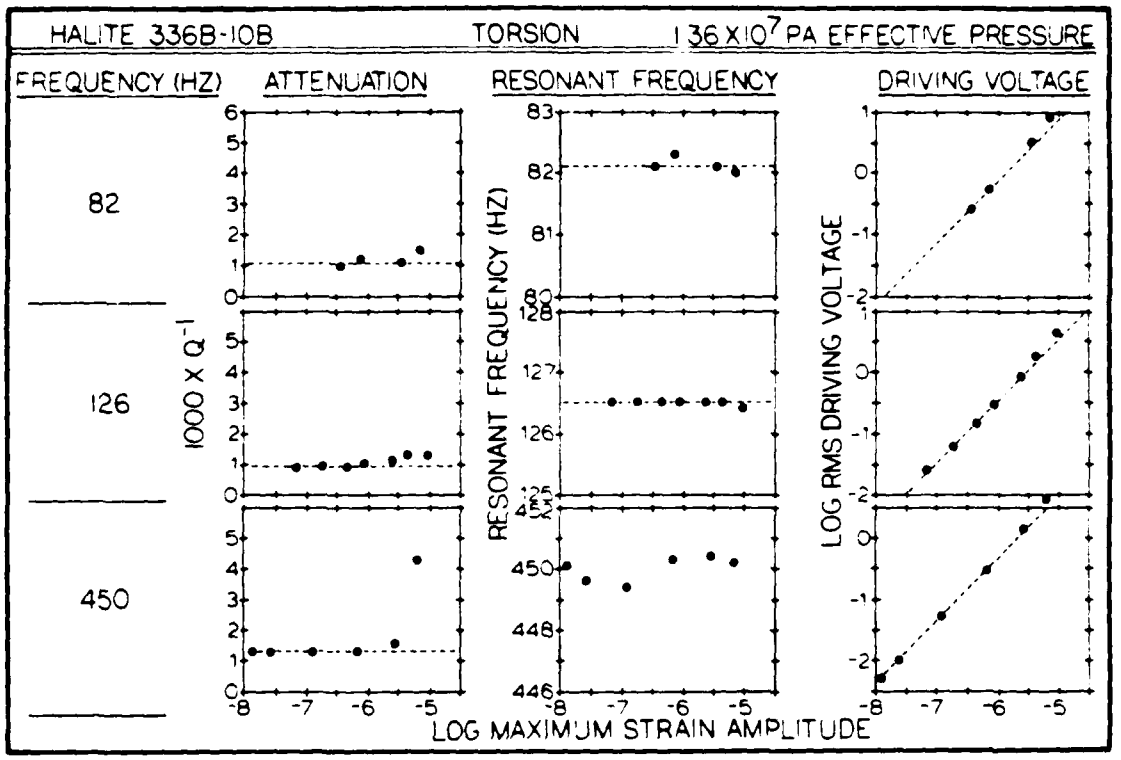

Fig. 21 Attenuation, resonant frequency, and log driving voltage plotted as a function of log maximum vibration amplitude for shear waves (torsion), and at several effective pressures up to 6.8×10^7 Pa.

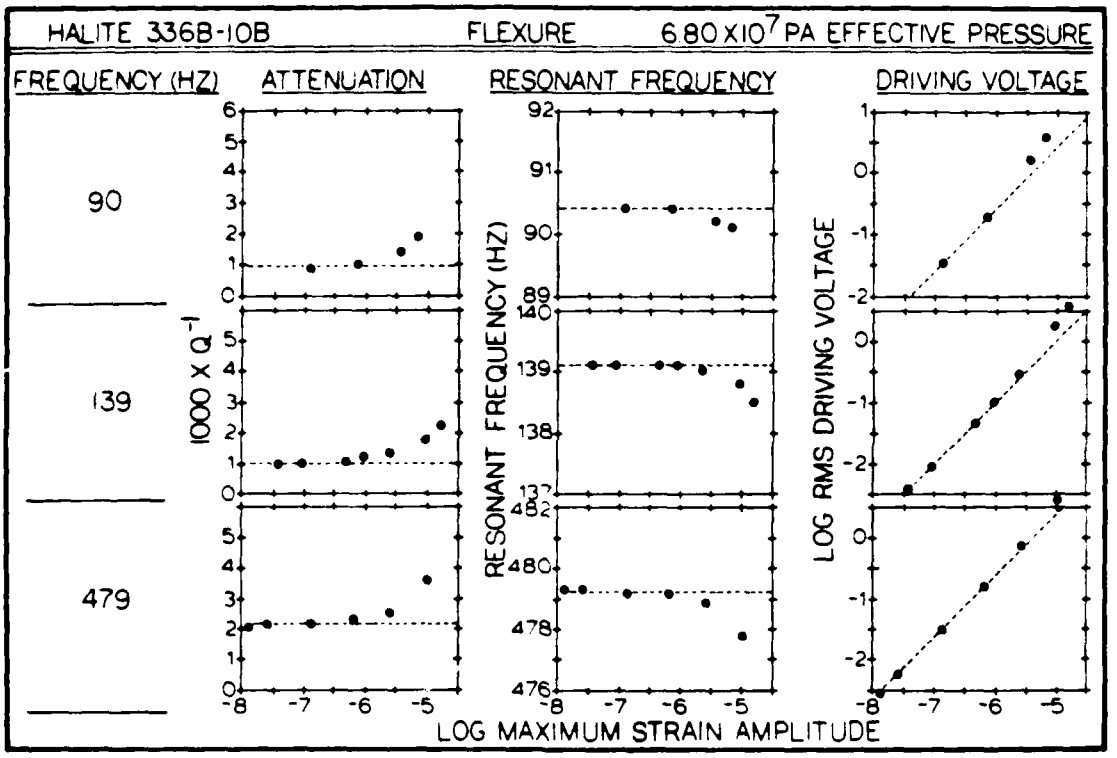

Fig. 22 Attenuation, resonant frequency, and log driving voltage plotted as a function of log maximum vibration amplitude for extensional waves (flexure) at 6.8 × 10^7 Pa effective pressure, and at several frequencies.

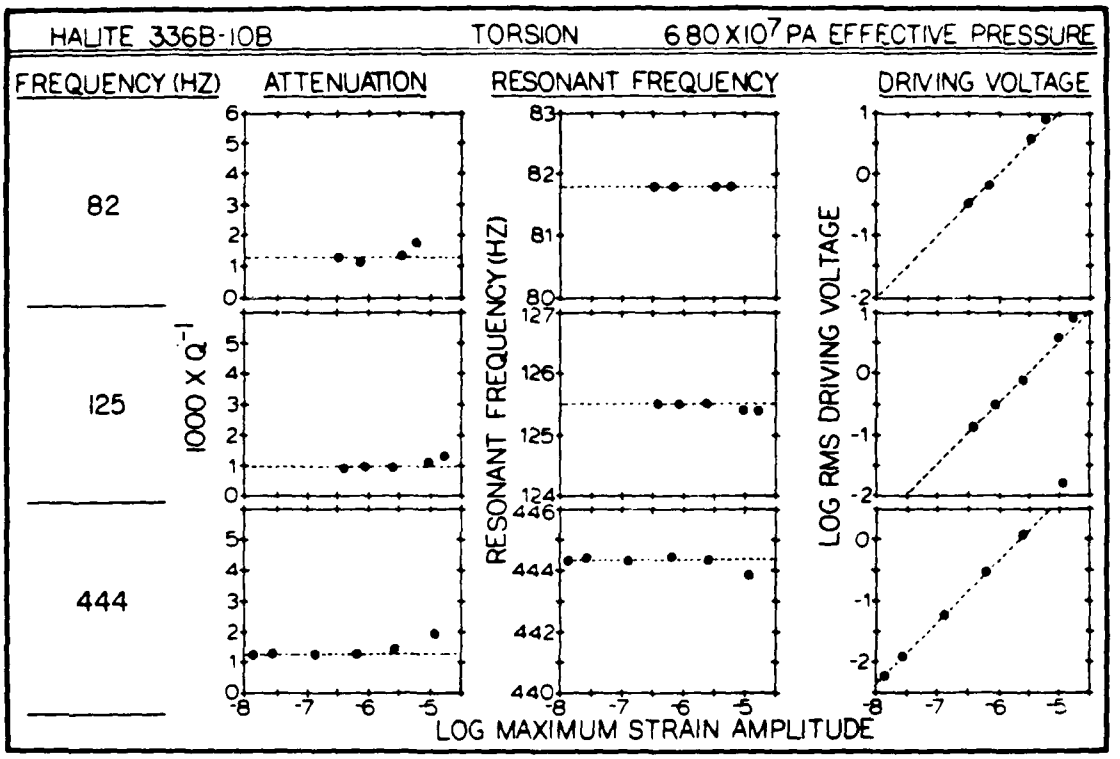

Fig. 23 Attenuation, resonant frequency, and log driving voltage plotted as a function of log maximum vibration amplitude for shear waves (torsion), and at several effective pressures up to 6.8×10^7 Pa.

5.0 DISCUSSION

The experimental measurements presented in this report indicate that elastic wave attenuation in pressed polycrystalline salt depends on frequency, humidity, effective pressure, and vibration amplitude. At any given strain amplitude, attenuation decreases with increasing frequency and increases with increasing humidity. The dependence on humidity suggests that attenuation may be related to slip along grain boundaires and cracks, with a coefficient of friction which is humidity dependent. An analysis of driving voltage, resonant frequency, and attenuation as a function of maximum vibration amplitude indicates that two domains of behavior are evidently present under ambient pressure conditions: 1) at low strain amplitudes ($<2 \times 10^{-6}$), attenuation is slightly amplitude dependent, indicating weakly nonlinear behavior, and 2) at high strain amplitudes ($>2 \times 10^{-6}$), attenuation is strongly amplitude dependent, indicating strong nonlinear behavior. By raising effective pressure, it is possible to raise the threshold amplitude for strong nonlinear behavior to greater than 3×10^{-5}.

Measurements on natural dome salt under ambient pressure conditions show that nonlinear behavior persists even at very low amplitudes (10^{-8}). With increasing effective pressure the threshold amplitude for nonlinear behavior increases to approximately 3×10^{-6}, corresponding to a stress of about 1 bar. It is noteworthy that the intrinsic linear anelastic Q for dome salt is very high compared with values reported by Trulio (1980) and Larson (1981), based upon near-field measurements.

In studies of particle motion associated with small-scale chemical explosions in pressed salt (Larson, 1981), an amplitude dependent attenuation was demonstrated at strains from 1.4×10^{-3} to 7×10^{-4}. A significant amount of dispersion was also observed. The Q values which Larson reports ($Q = 12.5$ over the strain amplitude range from 1.4×10^{-3} to 7×10^{-4} and $Q = 24.9$ from 7×10^{-4} to 4.6×10^{-4}) are much lower than those reported here for pressed salt at low amplitudes ($Q > 250$), confirming am amplitude dependent attenuation

indicative of nonlinear behavior at strain amplitudes near 5×10^{-4}. On the basis of free-field data from the Cowboy series, Trulio (1980) reports a Q value near 3 in the frequency band 0.5-5 Hz and in the distance range 0.75 - 4 km from the Salmon event. This value contrasts strongly with the high Q values reported in this study for natural salt in the linear regime.

In dome salt at about 100 Hz a Q value near 1000 is reported for both extensional (Young's modulus) and shear waves. A slight frequency dependence to the linear anelastic Q is suggested by measurements in the frequency range from approximately 80 Hz to 500 Hz. This will be explored more thoroughly in future studies.

While the resonant bar-type measurements are well suited for measuring attenuation and velocity in the linear anelastic regime, at least two other issues need to be considered before one can apply these high amplitude (non--linear) Q measurements to high amplitude seismic pulse propagation. The first of these involves the definition of strain amplitude. In this study we report measurements as a function of strain amplitude which is calculated at a position of maximum strain in the specimen. For torsional and flexural vibrations first order strains vary from zero to the value reported which is the maximum. Therefore the attenuation measurements reported do not represent values for incremental units of volume exposed to homogeneous strain. It is felt that a careful analysis of the stress field within the specimen will result in a solution to this problem. This issue will be pursued in follow-up studies.

The second problem is somewhat more subtle, and involves the response of the specimen to repeated cycles at very high nonlinear amplitudes. The test specimen may have a memory, in which case the first elastic pulse propagates through a material which has equilibrated with a more or less static environment for a relatively long time period. Each successive pulse passes through a material which has accumulated changes resulting from exposure to be previous pulses.

The forced resonance technique measures modulus and attenuation in a specimen which has reached a more or less steady state after exposure to a long

train of high amplitude pulses. High amplitude seismic wave trains are naturally of shorter duration. In future research programs nonlinear attenuation should be measured by watching the free decay in a system after one large initial pulse.

6.0 CONCLUSIONS

The experimental results described in this report indicate that natural dome salt is rather ideally behaved. At elevated effective pressures linear anelastic behavior is observed at strain amplitudes below about 2×10^{-6}, corresponding to stresses of about 1 bar. The linear anelastic Q for natural dome salt is quite high (~ 500 in extension and ~ 1000 in torsion), apparently independent of pressure up to 6.8×10^{7} Pa, and very slightly dependent on frequency between ~ 80 Hz and ~ 480 Hz. Nonlinear behavior, as reflected in an amplitude dependent Q, is observed at strain amplitudes above 2×10^{-6}, at all effective pressures to 6.8×10^{7} Pa (corresponding to burial depths of about 2.4 km). The observed departure from linear behavior in dome salt at strain amplitudes higher than 2×10^{-6} (~ 1 bar stress) indicates that RDP studies based upon particle motion measurements at higher amplitudes may not be useful for defining a seismic source function.

The behavior of pressed salt contrasts with that of natural dome salt. Weakly nonlinear behavior persists to very low amplitudes (below 10^{-8}), corresponding to stresses of approximately .01 bars. Strongly nonlinear behavior is observed at strain amplitudes higher than 10^{-6}. Attenuation in pressed salt is frequency dependent. Under ambient pressure conditions attenuation is also sensitive to the amount of moisture adsorbed on internal cracks within the sample.

The microstructure of both types of salt has been described. The most obvious difference between pressed salt and natural dome salt is in the grain size. The grains in the pressed salt are more than a decade smaller than the grains in the dome salt. This corresponds to at least a two decade difference in grain surface to volume ratio. These microstructural differences combined with the observed difference in the Q behavior of both types of salt cast suspicion on the use of pressed salt as a good mechanical analog for natural dome salt.

7.0 REFERENCES

1. Bache, T.C., W.J. Best, R.R. Blanford, G.V. Bolin, D.G. Harkrider, E.J. Herrin, A. Ryall and M.J. Shore (1981), a Technical Assessment of Seismic Yield Estimation, DARPA Report, January 1981.

2. Harbottle, J.E., 1970, An instrument for studying low frequency internal friction at constant amplitude in irradiated foils, Jour. of Phys. E: Scientific Instruments, 3, 49.

3. Johnson, W.A., 1946, Estimation of Special Grain Size; Metal Progr., 49, 87.

4. Johnston, D.H. and M.N. Toksöz (1980), Thermal Cracking and Amplitude Dependent Attenuation, J. Geoph. Res. 85, 937-942.

5. Larson, D.B., Inelastic Wave Propagation in Sodium Chloride, unpublished manuscript (1981).

6. Mavko, G.M. (1979), Frictional Attenuation: An Inherent Amplitude Dependence, J. Geophys. Res. 84, 4769-4776.

7. Saltykov, S.A., 1958, "Sterometric metallography," 2nd Edition, Metallurgist, Moscow, 446 p.

8. Tittmann, B.R. and J. Curnow, 1976, Apparatus for measuring internal friction Q factors in brittle materials, Rev. Sci. Instrum. 47, 1516.

9. Tittmann, B.R., M. Abdel-Gawad, C. Salvado, J. Bulau, L. Ahlberg and T.W. Spencer (1982), A Brief Note on the Effect of Interface Bonding on Seismic Dissipation, Proc. Lunar and Planetary Science Conf. 13th.

10. Trulio, J.G. (1978), Simple Scaling and Nuclear Monitoring, Final Report of DARPA supported research program, April, 1978.

11. Trulio, J. G. (1981), State-of-the-Art Assessment: Seismic Yield Determination, in A Technical Assessment of Seismic Yield Estimation, DARPA Report Appendix, January, 1981.

12. Underwood, E.E., 1968, Particle Size Distribution, in DeHoff, R.T. and Rhines, F.N. (Editors): Quantitative Microscopy," Chapter 6, McGraw Hill, p. 149-200.

13. Winkler, K., A Nur and M. Gladwin (1979), Friction and Seismic Attenuation in Rocks, Nature, 227, 528-531.